Hypersonic ReEntry Deployable Glider Experiment (HEDGE)

2023 - 2024 Academic Year Report

MAE 4700 Spacecraft Design II

Department of Mechanical and Aerospace Engineering
School of Engineering and Applied Sciences
University of Virginia

ADVISOR
Christopher Goyne
Department of Mechanical and Aerospace Engineering

April 24, 2024

TEAM MEMBERS:

Temidayo Akinbi	Samuel Falls	Timothee Kambouris	Owen Solomon
Katie Borland	Jennifer Farfel	Emmanuel Kenscoff	Tyler Spittle
Justin Carroll	Isaac Farias	Benjamin Koeppen	Owen Tuohy
Arlee Christian	Brandol Galicia	Ian McAninley	Kate Wilkins
Juan Victor Corsino	Rishab Gopisetti	Morgan Myers	Najarie Williams
Troy Daigneau	Lucas Haddock	Amy Paz Cuervo	
Lobsang Dawa	Sean Jolly	William Plunkett	
Griffin Dewey	William Jones	Brett Schriever	

Proposed period of performance for follow-on project:
April, 2024 - March, 2027

Approved by: C.P. Goyne, April 26, 2024

Table of Contents

Introduction

Background and Context

The Department of Defense has identified hypersonics, "as one of the highest priority modernization areas," since the United States has fallen behind other nations in the development of the technology (Vergun, 2021). Hypersonic technology has both military and civilian applications due to the associated high speed and maneuverability over conventional aircraft. A CubeSat is a small satellite that can be launched as a secondary payload as a part of another spacecraft launch. CubeSats can therefore be launched relatively inexpensively, and may incorporate many commercial off-the-shelf (COTS) parts. This team of undergraduate students aims to utilize a CubeSat form-factor to conduct a hypersonic glider experiment. Proving that hypersonic flight experiments can be conducted by a team of undergraduates using a CubeSat would be an advancement in the field of hypersonics testing.

The Hypersonic ReEntry Deployable Glider Experiment, or HEDGE, is a proof of concept mission to demonstrate the feasibility of using CubeSats as a means of low cost sustained hypersonic flight. Created and designed by University of Virginia aerospace and mechanical engineering undergraduates, HEDGE will demonstrate the ability of undergraduate students to perform hypersonic experiments at lower cost and with greater accessibility than traditional programs. Currently, the design of HEDGE is being finalized, while prototyping is being conducted to ensure that HEDGE will be able to function as designed during its mission. This document begins with the general project overview and mission statement. Below are the objectives, both primary and secondary, that have been outlined by the program team from the initial year. Continuing on in the document, the concept of operations of HEDGE is outlined in Figure 1, as well as a breakdown of class organization and team roles. A breakdown of the budget and schedule follows. Each subsystem design group's accomplishments and plans for the future are discussed, and an overall path forward is highlighted.

Mission and Project Overview

Mission Statement:

The purpose of this mission is to demonstrate the feasibility of using CubeSats in low cost hypersonic glider flight experiments.

Mission Objectives:

Table 1 contains the Primary and Secondary Mission Objectives for HEDGE.

Table 1: HEDGE Mission Objectives

Primary Mission Objectives	Secondary Mission Objectives
Demonstrate the feasibility of inexpensive CubeSats as	Expose undergraduate students to best practices of

a platform for hypersonic glider flight research	industry, government, and research professionals
Demonstrate a materials screening method at hypersonic flight conditions at a low cost	Connect undergraduate students with aerospace professionals
Demonstrate that undergraduate students are capable of conducting hypersonic flight experiments at lower cost and with greater accessibility than traditional methods	Give undergraduate students hands-on experience working on a complex design-build-fly project

Concept of Operations:

The concept of operations for a representative HEDGE flight into Low Earth Orbit (LEO) is detailed in Figure 1.
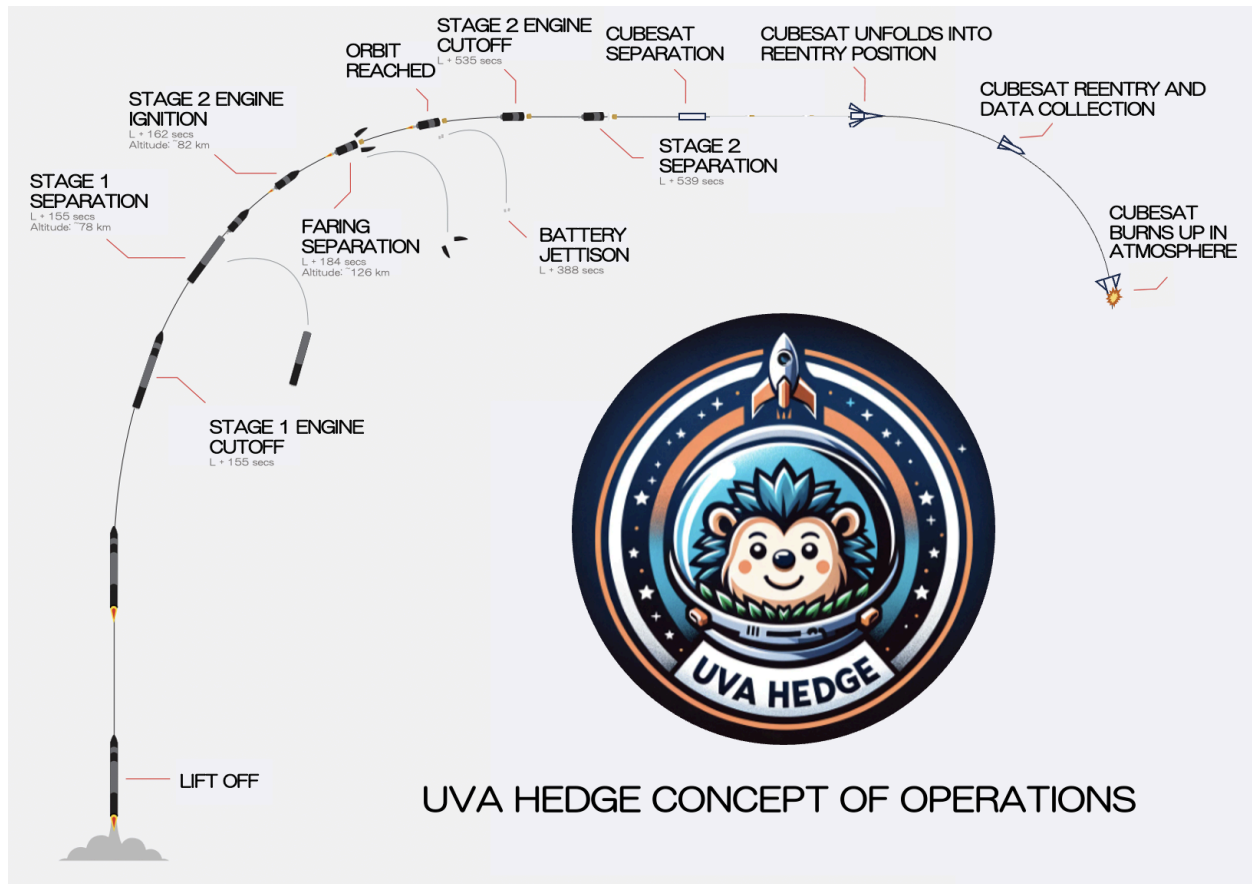

Figure 1: HEDGE Concept of Operations Adapted from "Payload User's Guide", 2022

Design Requirements and Constraints:

Tables 2, 3, and 4 detail Functional and Operational Design Requirements and Mission Constraints for a HEDGE flight.

Functional Design Requirements:

Table 2: Functional Design Requirements Table

F1	Hypersonic vehicle fins must autonomously be in deployed position during reentry
F2	Aerodynamic stability with correct orientation required during reentry
F3	Withstand launch and orbit conditions and environment
F4	Sustain hypersonic flight during data transmission
F5	Conform to launch provider requirements
F6	Ability to accommodate different material test panels on the Outer Mold Line

Operational Design Requirements:

Table 3: Operational Design Requirements Table

OP1	Less than 16 day orbital lifetime
OP2	Automated, powered system to control data collection and telemetry (including temperature and pressure measurements)
OP3	Test article must survive data collection but demise prior to impact

Mission Constraints:

Table 4: Mission Constraints Table

C1	Comply with CubeSat Standards	1.3U maximum size 2.Total mass < 6 kg
C2	Launch to Extreme Low Earth Orbit (ELEO)	~200 km Altitude
C3	Cost consistent with student flight programs	< $100,000
C4	Comply with FCC and launch provider regulations for space communications	

Program Management

Budget:

     The projected budget to build one HEDGE vehicle is ~$72,750. This value includes the costs of parts, and materials and supplies. Labor, such as summer student internships and graduate student stipends, and travel costs, are not included. A full, detailed budget is shown in Appendix B.

Schedule:

        A schedule for HEDGE from Fall semester 2023 through a HEDGE-2 flight and analysis is shown in Table 5. HEDGE-0 will be a prototype flight vehicle for testing purposes. HEDGE-1 will be the first generation to be launched, followed by HEDGE-2. The TIM was conducted in the Fall of 2023 and the CDR is scheduled to take place in April 2024. Therefore, HEDGE is on schedule as of the time of this thesis.

Table 5: HEDGE Schedule

Schedule (calendar year)	2023		2024				2025				2026				2027	
	Q3	Q4	Q1	Q2	Q3	Q4	Q1	Q2	Q3	Q4	Q1	Q2	Q3	Q4	Q1	Q2
Contracting	■	■	■	■	■	■	■									
Part selection and Technical Interchange Meeting (TIM)	■	■														
Critical Design (CDR)			■	■												
Systems Integration (SIR)					■											
Fabricate HEDGE-0 Prototype					■	■										
Test Readiness Review (TRR)							■									
Flight Vehicle Lab Testing							■									
HEDGE-0 Complete and Report							■									
HEDGE-1 Preflight Environmental Testing								■								
Flight Readiness Review and Launch Vehicle Integration									■							
HEDGE-1 Flight									■							
HEDGE-1 Data Analysis and Report									■	■	■					
HEDGE-2 Fabrication and Testing (FRR)												■	■			
HEDGE-2 Flight														■		
HEDGE-2 Data Analysis and Report															■	■

Management Approach:

The Program Management team is responsible for ensuring that HEDGE has the best chance of meeting all mission objectives through effective cooperation between functional teams. The main job of this team is to ensure effective communication between groups, keeping the project on schedule and budget, and keeping a record of tasks across the class. This leads up to the completion of a Critical Design Review (CDR) at the end of the Spring semester. The completion of this meeting will demonstrate that the HEDGE project is ready for assembly, which will be a task that next year's HEDGE capstone class will take on.

The class has been broken up into six subgroups, which can be found in Appendix A, and include Program Management, Communications, Software and Avionics, Power, Thermal and Environment, Attitude Determination and Control Systems (ADACS) and Orbits, and Structures and Integration. These groups meet twice a week in class to work with the other members of their subgroup and coordinate across groups and with the Program Management team.

Federal Communications Commission (FCC) Licensing:

An experimental license from the FCC's Office of Engineering and Technology (OET) will be required for HEDGE to communicate to Iridium. This will need to be requested through the Special Temporary Authorization (STA) application process, which is meant for experiments lasting less than six months. The OET recommends filing no later than 30 days prior to the desired start date of the license, as applications are processed on a first come, first serve basis. However, it is also recommended that the application be submitted no later than 90 days prior to launch vehicle integration (OET, 2013). As demonstrated with TechEdSat-1, a joint experiment with NASA and numerous universities, a license needs to be approved prior to launch. TechEdSat-1 did not receive approval prior to launch vehicle integration, and thus had to disable its Iridium transceiver to proceed with launch (Riot et al, 2021).

The space community, based on best practices and lessons learned, has determined that it is best to start the application process a year in advance (S3VI, 2023). A year will allow changes to be made and address any issues the FCC has if the initial application is rejected. As previously stated, applications are processed first come, first serve, thus if the application is rejected, it is reasonable to expect a new application with changes to take a comparable amount of time to process as the initial application. For a tentative Q3 2025 launch for HEDGE-1, the STA application should be started no later than Q3 of 2024 to allow for potential changes if the FCC rejects the initial application.

The process for completing the STA application along with a preliminary schedule is located in Appendix I. An account has been created through the FCC's Commission Registration System (CORES), and a FCC Registration Number (FRN) has been assigned. The FRN is required to begin the STA application process.

Risk Management:

A selection of identified potential risk items is detailed in Figure 2. Risk Scores are based on subteam-level assessment of the potential risk probability and impact on the mission.

Risk	Risk Score (Probability of occurrence x impact on mission)	Mitigation
Heat shield blocks signals from HEDGE to Iridium	20 (4 x 5)	- Conduct tests to better understand the signal's ability to penetrate the inconel heat shield, and relocate the antenna if necessary
HEDGE fin deployment mechanism will not deploy or hold fins in place as intended	15 (3 x 5)	- Conduct ground tests of the fin deployment mechanism to ensure robustness
Wired Connections Fail	12 (3 x 4)	- Shield electronics and soldered wires from the heat as much as possible
Unstable reentry	12 (3 x 4)	- Complete CFD simulation with up-to-date CAD models with accurate center of gravity and pressure to better understand HEDGE's stability
Fin Hinges burn up rapidly upon reentry	10 (2 x 5)	- Complete CFD and FEA simulations to get a better idea of the survivability of HEDGE

Figure 2: Risk Analysis (Scale in Appendix B)

As shown in Figure 2, there are two substantial risks to this mission. The first major risk is that the fin deployment mechanism will not properly deploy or hold fins in place as intended. This could be a result of the hinges breaking during reentry from excessive heat or just being ineffective in the first place. This risk can be mitigated by completing ground testing and analysis of the hinge mechanism in various conditions to ensure proper deployment. Another major risk is that the heat shield will block signals from being transmitted from HEDGE to Iridium. Many tests will be conducted on the ground to improve our understanding of this issue and to find ways to mitigate the risk to the mission. An example is relocating the antenna or altering the choice of antenna model for this mission. Some additional risks were identified, but corresponded to lower risk scores than in Figure 2.

Structures and Integration

Subsystem Level Constraints

The system must be able to withstand the aerodynamic and launch forces it will experience. It also needs to maintain aerodynamic stability by ensuring the center of pressure is behind the center of gravity, providing an adequate static margin during reentry as shown in Figure 3. The test vehicle must be capable of enduring the extreme hypersonic and flight conditions during its data transfer window. Additionally, both the vehicle and frame deploying it

must burn up in the atmosphere after the flight concludes. All communication and computing equipment, as well as the deployment mechanisms, need to be housed within the confines of a 3U CubeSat measuring 10x10x30 cm, with the entire system weighing less than 6 kg. Assembly of the spacecraft must be possible in-house without the need for specialized tools, and it must be compatible with the launch provider's dispenser. The frame must allow for deployment of the fins and the support material test panels and sensors.
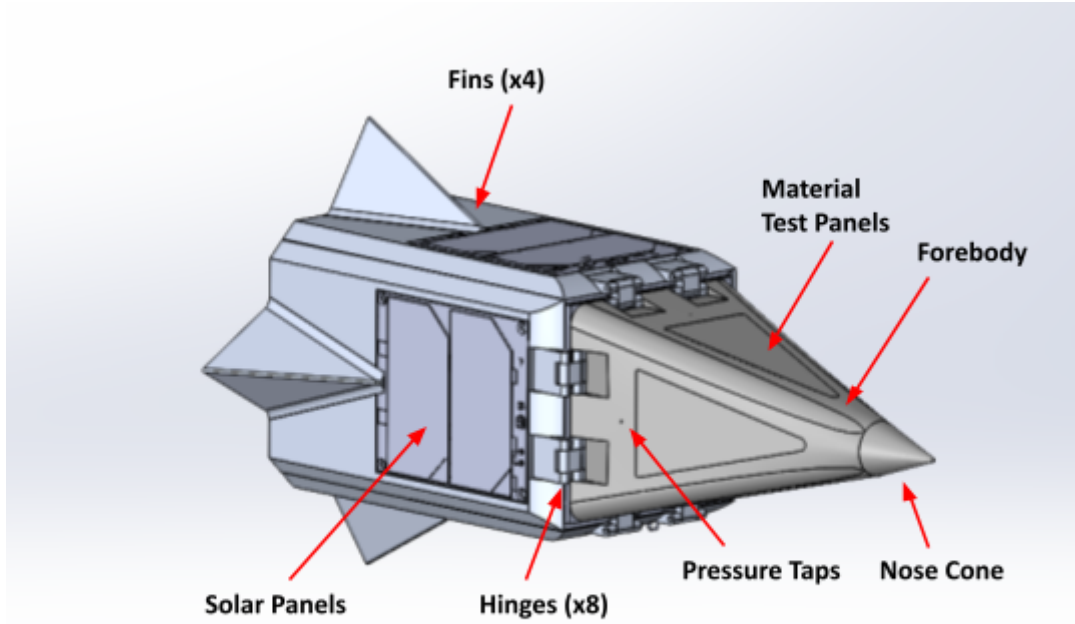

Figure 3: Spacecraft in re-entry configuration

Component Overview

The structure of the spacecraft consists of nine main components: Fins, Hinges, Forebody, Nose Cone, Test Panels, 1U CubeSat, 1U Side Plates, 1U Back Plate, 1U Front Plate. There are four fins attached to the forebody using double jointed hinges. The forebody is attached to the front plate and the 1U structure. At the tip of the forebody is the nose cone, which will be screwed on to a ballast weight that is placed within the forebody. The test panels are placed on each four faces of the forebody and are used to conduct material testing. There are six plates surrounding the 1U CubeSat, which are used for protective and mounting purposes. The front plate covers the face positioned toward the forebody and the back plate is facing the back of the spacecraft, and has the antennas externally mounted.

Fins and Solarpanels

The assembly was updated with the accurate models of the solar panels, and adjustments were made to the fins to accommodate the new solar panels. The first update made was to increase the thickness of the fin plates to allow the solar panels to fit into the previously designed

compartments. The shape of the compartments also had to be adjusted slightly to match the shape of the new solar panels. Holes were added to the fin plates for the purpose of fastening the solar panels to the fin plates. The solar panels will be electrically connected to the internal battery using magnetic connectors. One side of the magnetic connector will be on the inside of the fin plate and one on each of the side plates on the sides of the 1U cubesat. There will be one pair of connectors for each of the solar panels.

Figures 4, 5, and 6 give a better view of selected HEDGE components. The shape of the fin plates also had to be adjusted to accommodate the addition of the side plates onto the bus. The chamfered side edges of the fin plates were extended to make contact with each adjacent fin plate. This was completed with the intention of reducing the amount of hot flow entering the volume where the antenna is attempting to send communications. Appropriately sized cuts were made in the fin plates and side plates to accommodate the magnetic connectors. The cuts will allow the connector to fit into the cuts and sit flush with the surfaces that will contact each other: the bottom surface of the fin plate and outside surface of the side plate.
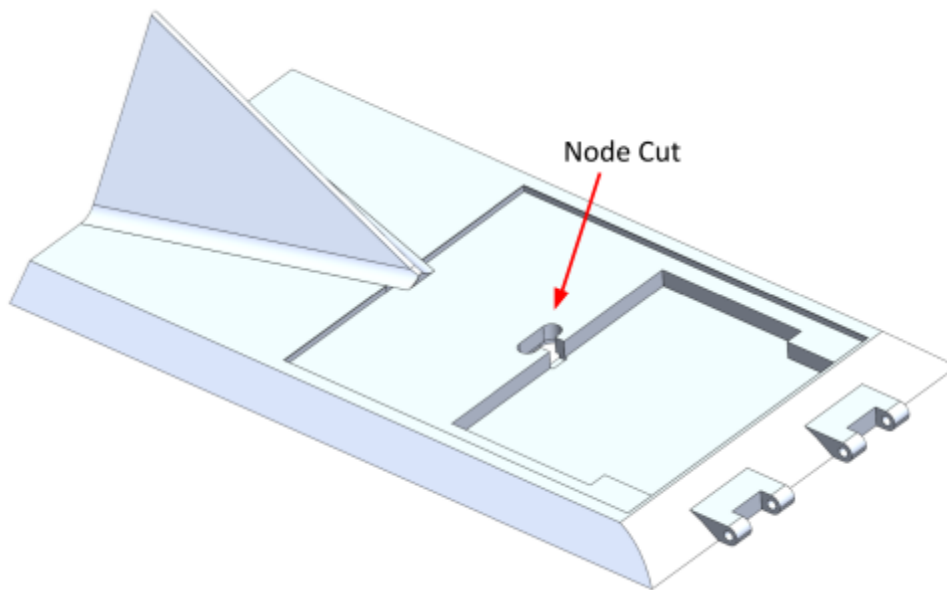

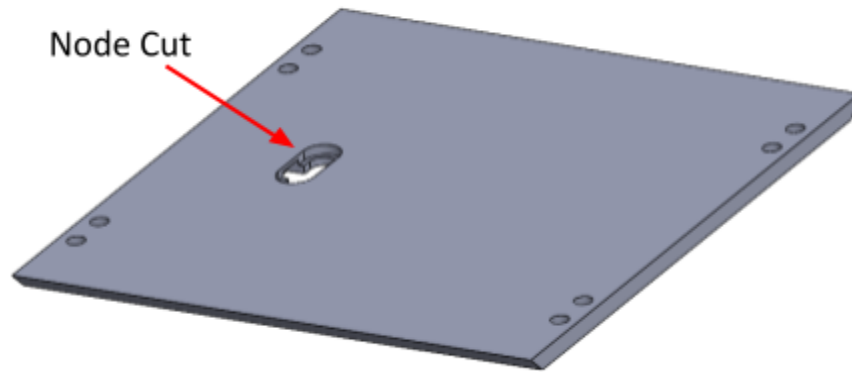Figure 4: Fin Plate Post-Updates with Node Cut Indicated

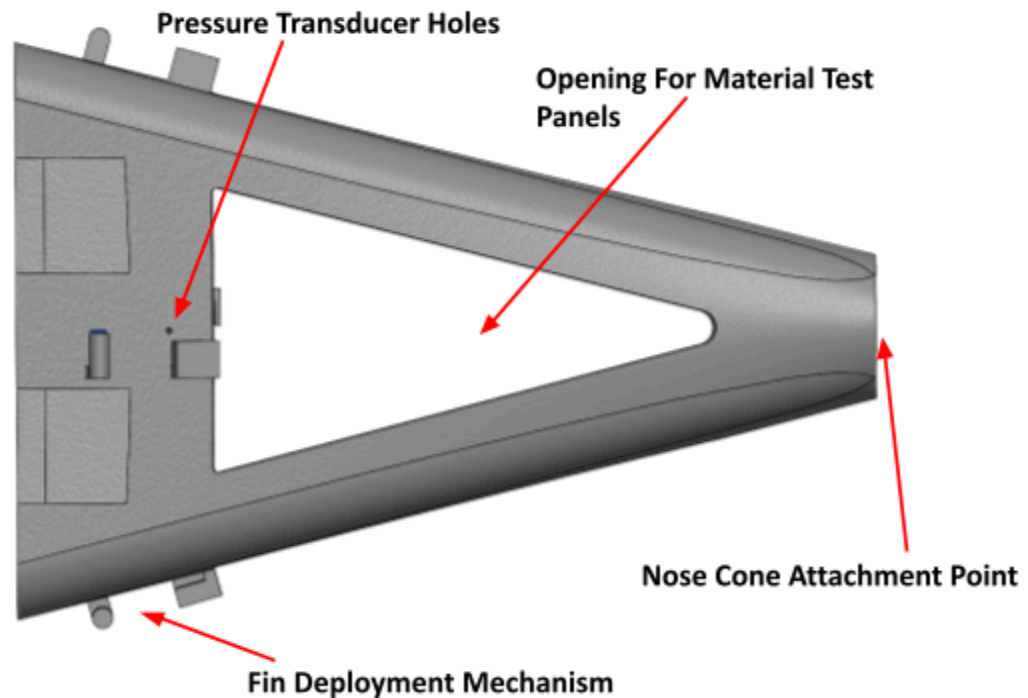Figure 5: Side Plate with Node Cut Indicated

Forebody

Figure 6: Forebody Diagram with spring holder

Hinges

A pair of double pin hinges on each of the four sides of HEDGE will connect the forebody to the fin plates. Each of the eight hinges are made up of the forebody hinge connector, the hinge center, the hinge pins and the fin plate hinge connector. These parts come together in order to allow the fins to lay flat and maintain the 3U size constraints while the spacecraft is in its undeployed configuration. This hinge design also allows the fins to open up and lay on top of the

1U CubeSat as it deploys into the re-entry configuration. The reason that a pair of hinges was decided over a single hinge is due to the aerodynamic and stability benefits of the double hinge vs a singular hinge.

Fin Plate Deployment Mechanism

A small torsion spring located between the two hinges on each side of the spacecraft is the mechanism used to deploy and open the fins of the CubeSat after it is released from the deployment box. These torsion springs will be located on the outside of the forebody and will wrap around a cylinder that will hold the spring in place. The spring will help to provide a force outwards against the inside of the deployment box. This pressure will prepare the CubeSat for deployment so that once the spring releases the fins will be in the proper configuration for flight and re-entry.

Antennas

The antennas used in the design are shown in Figure 7 below. The GPS/GLONASS and Iridium Screw Mount Embedded Dual Antenna (2JP0133BGF) offers a 2-in-1 configuration, and the hemispherical radiation pattern provides a full range connectivity between 1575 MHz - 1627 MHz frequencies. This embedded dual antenna offers an alternative solution where communication devices cannot use external antennas. This is relevant due to the environmental conditions that our vehicle will be experiencing. This is also the reason for the antenna's rear placement, to help mitigate the effect of the extreme conditions experienced during hypersonic flight, such as high temperatures and plasma, and also for improved signal strength/greater possibility of line-of-sight communication with the Iridium satellite constellation.
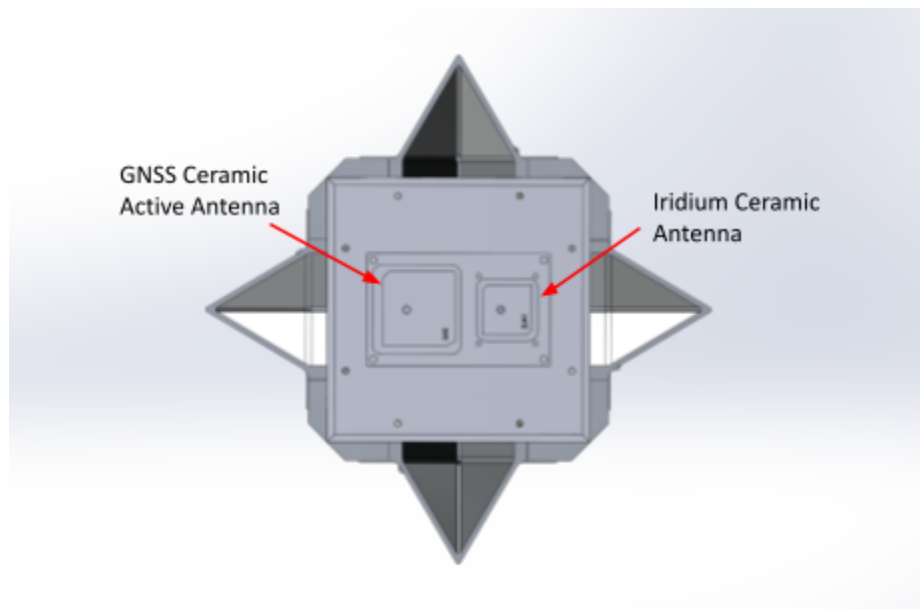

Figure 7: Antennas Located on Back of Spacecraft Bus

Internal Layout

   The internal components contained within the vehicle are the RockBlock Board, ADC Board, Iridium EPS, Iridium OBC, a weighted ballast, a battery cell, pressure transducers, and thermocouples. The internal layout of all the boards shown below in Figure 8 was determined by analyzing the direction of both the male and female pin connectors, and deciding what is most intuitive for allowing the connectors to be easily accessible for wiring. For example, the EPS only has one set of connectors on its front face, which indicated to us that it would have to go on the very back or very front side facing inwards, so that other internal connectors could then easily attach to it. Also contained on the inside of the vehicle is a weighted ballast, attaching to the back of the nose cone, and a battery cell that is stored within the forebody. The ballast was designed by the previous year's class in order to shift forward the center of mass to help maintain stability and ensure that the vehicle would have a nose down configuration during reentry. The forebody is hollow, and thus provides adequate room to house the battery cell to power the vehicle. It sits directly behind the nose cone and ballast and is screwed in place to secure it Pressure transducers and thermocouples are mounted to holes in the forebody as seen in Figure 7 above.
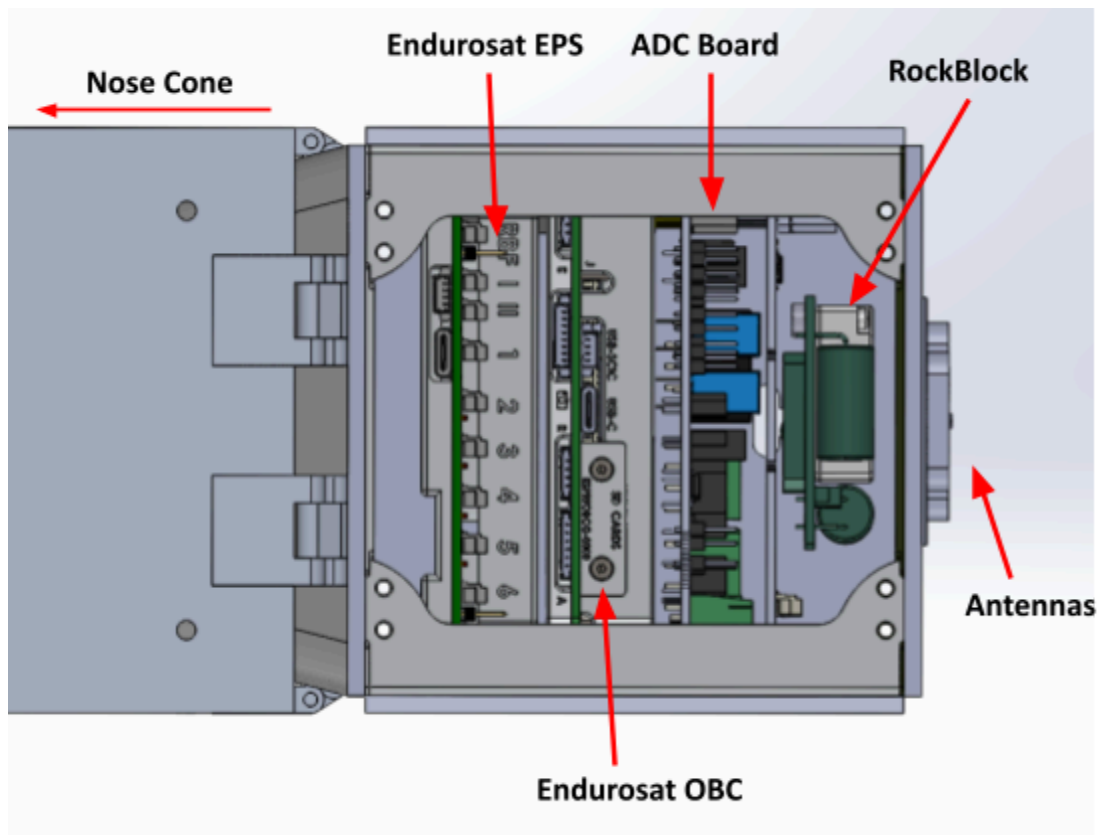

Figure 8: HEDGE Internal View, Fins not yet Deployed

Analysis Results and Prototyping

Design and analysis of the re-entry vehicle was carried out using Solidworks for CAD, and ANSYS, a simulation and 3D design software, to complete Finite Element Analysis and simulate the behavior of the vehicle under the anticipated hypersonic flight conditions. An iterative modeling approach was taken to improve upon last year's design through refinement. As the design is being finalized, 3D printing of a plastic prototype assembly is underway. The decision to incorporate new hardware components required adjustments to the design. The solar panels, for example, have pin connectors on the bottom that protruded farther into the depth of the fins than anticipated, and required adjustment.

Structural analysis has been completed on ANSYS to determine the structural ability of the spacecraft during reentry. During re-entry, the spacecraft is subjected to three pressures: ambient pressure, pressure after oblique shock, and pressure after an expansion fan.

Figure 9 depicts the flow around the contour of the craft. The flow passes from region 1 through an oblique shock to region 2. After reaching the top of the upwards slope, the flow forms an expansion fan and moves to region 3. The three resultant pressures were found using the Virginia Tech Compressible Flow calculator and the Prandtl-Meyer Table and were applied to the regions of the model shown below in Figure 10. Calculations for these values are provided in Appendix E.

$P_1 = 1.1$ Pa
$M_1 = 20$
$T_1 = 198.64$ K

18.03°

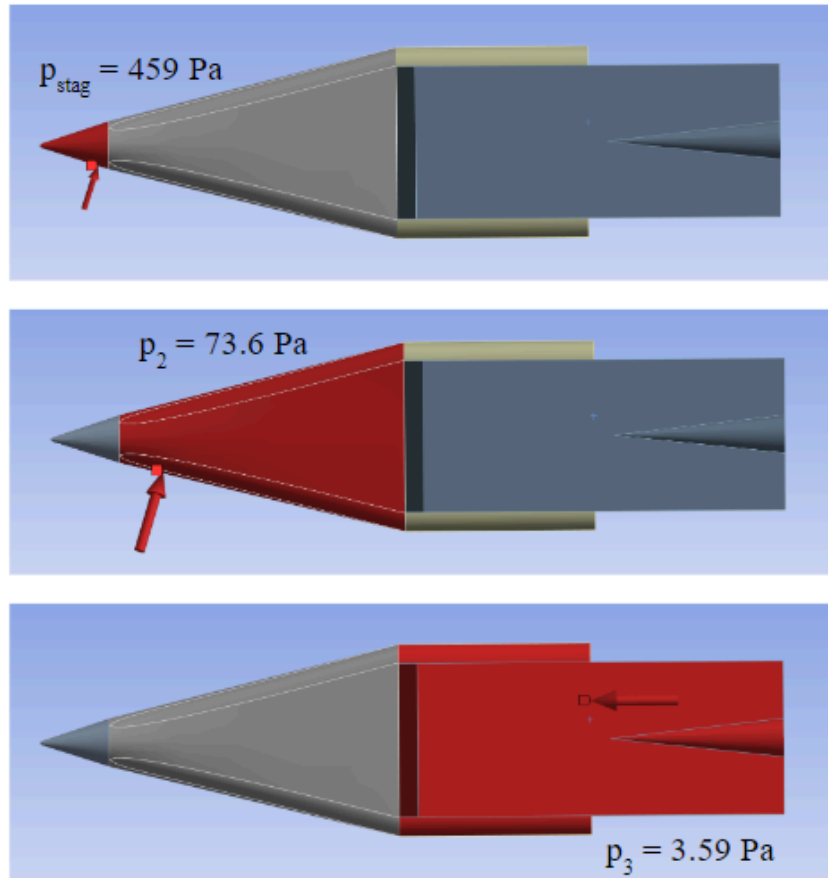Figure 9: Oblique shock followed by expansion fan

Figure 10: Pressure boundary conditions in ANSYS

Thermal loads were also calculated and applied to the model to derive both a transient thermal and transient structural solution within ANSYS. These thermal loads, initial temperature, convection, and radiation, are derived and displayed in the Power, Thermal, and Environment section: *Prototyping and Analysis: Thermal* and in Appendix E. Thermal and structural boundary conditions are displayed in Appendix G.

Mass Budget

The mass contributions from each subsystem are listed in Appendix J. The total mass of the system is required to be under 6,000 g. The total vehicle mass is 5,738.01 g. The increase in mass is due to recent extrusions of the fins and the switch from teflon to inconel test panels. The mass of the ballast may be decreased and some material may be cut away at the tail end of the fin to ensure the system remains under 6,000 g. The center of mass is located 199.52 mm from the tip of the nose cone along the centerline.

Software and Avionics

Subsystem Level Constraints

The Software and Avionics subsystem is anchored by the onboard computer (OBC), which orchestrates data processing and manages the spacecraft's central operations. Tasked with interfacing with the Iridium transceiver for data transmission and interacting with the attitude determination and control system (ADACS) subsystem and power, thermal, and environment (PTE) subsystem for power distribution, the OBC is the mission's linchpin. It holds the critical software that executes functions ranging from initiating wake-up protocols to managing and sending sensor-acquired data. The Software & Avionics design requirements are listed as follows:

1. Radiation Hardening: The OBC must withstand the intense radiation environment of Extreme Low Earth Orbit, ensuring reliability throughout the mission.
2. Re-entry Endurance: Operation within a re-entry environment, where the OBC will face high vibrational and thermal loads, significant vibration, and extreme temperature shifts.
3. Data Processing Capacity: Adequate RAM speed and solid-state drive performance to swiftly process and store the collected data during the mission's flight phase.
4. Size Constraints: All electronic components, including the OBC, must be compact enough to fit within the limited space of a 1U CubeSat structure.

Fulfilling these requirements ensures that the OBC can effectively manage the mission's critical operations, from the initial wake-up commands to the final transmission of data back to Earth.

The Global Navigation Satellite System (GNSS) receiver's role in relaying mission data such as position, altitude, and velocity is crucial when the CubeSat is in the orbital and reentry phase. However, its significant power consumption threatens the mission's efficacy. Precise control over the GNSS's operational state—specifically, its strategic activation and deactivation—is essential to prevent undue power depletion that could compromise the CubeSat's functions. The receiver is built into the Endurosat OBC and must be enabled / disabled through specific pins on the Endurosat bus. Although EnduroSat has not yet confirmed it, this functionality is crucial due to power budget considerations and therefore must be achieved somehow. During both the orbit and re-entry stages, vital temperature and pressure readings will be gathered in addition to the GNSS data. These measurements are taken by thermocouples and pressure transducers, which must operate reliably within specified temperature ranges under the extreme conditions of hypersonic re-entry. Simultaneously, these components are constrained by the CubeSat's 1U volume limit, posing a challenge for spatial efficiency.

The Analog to Digital Converters (ADCs) are entrusted with converting raw sensor data into digital packets. Their efficiency and accuracy are paramount; any failure to convert data swiftly would result in a bottleneck at the moment of transmission. This process is further complicated by the OBC's limited storage capacity of 3,000 megabytes and the stringent

transmission limit of 340 bytes per burst to the Iridium network. In anticipation of potential data transmission constraints—especially if the connection to the Iridium network is temporarily lost during the critical hypersonic re-entry—a hierarchy of data priority must be established. This hierarchy will guide the decision-making process for data retention or deletion, ensuring that, upon re-establishing a connection, the most valuable data is transmitted first, while continuing to collect new data. The implementation of this hierarchy is not just a matter of technical necessity but a strategic imperative for the mission's success.

Component Overview

        The main components that go into the software and avionics of HEDGE are as follows: the onboard computer (OBC), an electric power system (EPS), a GNSS receiver, four thermocouples, four pressure transducers, and analog-to-digital converters (ADC). The OBC is a central processing unit that interfaces with the other subsystems in HEDGE such as the power, thermal, and communications systems. It internally performs data handling and transmission. The EPS is a combination of electrical components that manages and transfers power to all the other avionic components. The GNSS receiver will provide GPS functionality to locate the spacecraft while also providing altitude and velocity data. The thermocouples and pressure transducers will collect temperature and pressure data, respectively. These components will transmit a signal as an analog voltage; therefore, the ADCs will be used to convert that voltage to a digital input.

        The components were chosen based on the data that needs to be processed and their ability to withstand flight conditions. The OBC that will be used is the Endurosat OBC because it has flight heritage. According to the NASA Small Spacecraft State of the Art Report, the Endurosat OBC has a technology readiness level of 9, meaning that the OBC has been through successful mission operations. (Weston, 2024) Sticking with Endurosat, the EPS that will be used is the Endurosat EPS because of its low power consumption and four plus years of flight heritage. The 2JP0133BGFz Iridium Patch Antenna is a 2-in-1 combination antenna that will be mounted at the aft of the craft. It has an Iridium antenna that communicates, transmits, and receives data through the Iridium constellation. It also has a GNSS antenna receiver that will receive real-time positioning data. The chosen thermocouple and pressure transducer are the Omega Inconel Type K Thermocouple and the Kulite XCE-80 pressure transducer. These components were chosen because their temperature ranges are within the predicted HEDGE temperature constraints. The MAX 6675 ADC for the thermocouple and the MAX 11254 ADC for the pressure transducer were chosen because their electric characteristics allow them to directly interface with the chosen sensors and are easily mountable on a PCB.

        The selected components have been replaced with stand-in components for the benchtop prototype that was completed this semester. The stand-in components are used because the mission's finalized OBC, thermocouples, and pressure transducers had not yet arrived at the time of preparing this document. These stand-in components are essential to developing the software architecture. The NUCLEO L476RG board will be the stand-in OBC because it utilizes the same

ARM-7 microchip as the Endurosat. The GPS module PA1616D is used as a stand-in. The stand-in thermocouples (Type K Fiberglass KBB) and pressure transducers (MEAS Press XDCR M3021-000005-10KPG) were used because of price, availability, and ease of use. Figure 11 shows the benchtop prototype.
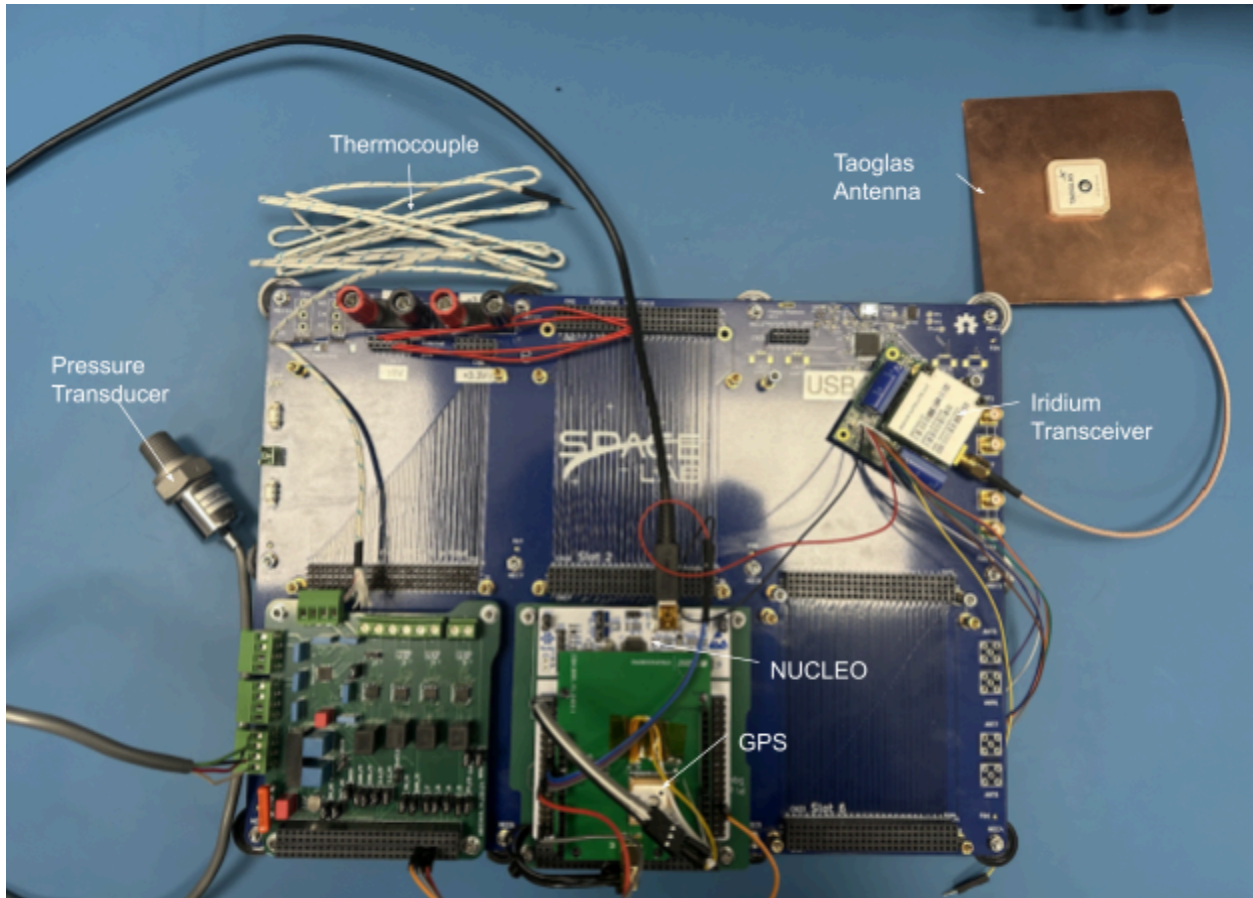

Figure 11: Photograph of the FlatSat with major components labeled

Prototyping and Analysis

Two printed circuit boards were designed and built, with the help of electrical engineering capstone students. These boards are designed in such a way that allows them to be stacked and fit in the 1U cubesat frame. One board is for the Iridium transceiver and the other board is for the thermocouples and pressure transducers. However, complications with the Iridium transceiver board has resulted in using a ROCKBlock. The ROCKBlock is a manufactured printed circuit board that already has the Iridium transceiver on it.There will be four pressure transducers and four thermocouples located on the forebody of the cubesat. There will be one thermocouple under each test panel to measure the temperature of the test material during reentry. Once necessary wiring is completed, the circuit boards will be able to interface with the OBC and transmit data. The pressure transducers require external power so there will be

lead wires that attach to the EPS system. Meanwhile, the thermocouples do not require any power supply

     As mentioned above, for prototyping purposes a NUCLEO L476RG development board was used in place of the Endurosat OBC. The boards were placed on a flatsat for hardware testing and software development. In STM32CubeIDE, an integrated development environment for STM32, we developed code in C/C++ to carry out tasks shown in Table 4. The final design and prototyping have the same functions, however for the final design we will use FreeRTOS and NASA CFS. The softwares are frequently used in the spacecraft industry and have flight heritage, making them reliable for data transmission for the final HEDGE design.

Table 4: General Tasks for Software and Avionics

General Tasks		
Task	**Description**	**Relevant Components**
Clocking	Allow data collection and transfer to occur at exact and repeating timestamps.	OBC
Data Collection and Handling	Enables the system to collect necessary data from the sensors, and process them in order to export comprehensible data.	OBC, MAX6675, Kulite-X80, MAX11254, Inconel Type K
Transfer Data	Enables the system to export data to the Iridium satellite constellation.	OBC, RockBLOCK 9603 Transceiver

     Figure 12 shows the data distribution within HEDGE. As mentioned, the EnduroSat OBC is the onboard computer and will have flight software that collects data from the pressure transducer, thermocouple, and EPS and transmits data through Iridium transceiver. The pressure transducers and thermocouples signals will be transferred to the OBC through SPI data transfer protocols. The EPS board will be connected through I2C. The Iridium patch antenna will be connected through UART, and the Iridium ISU connects to the OBC through API and UART.
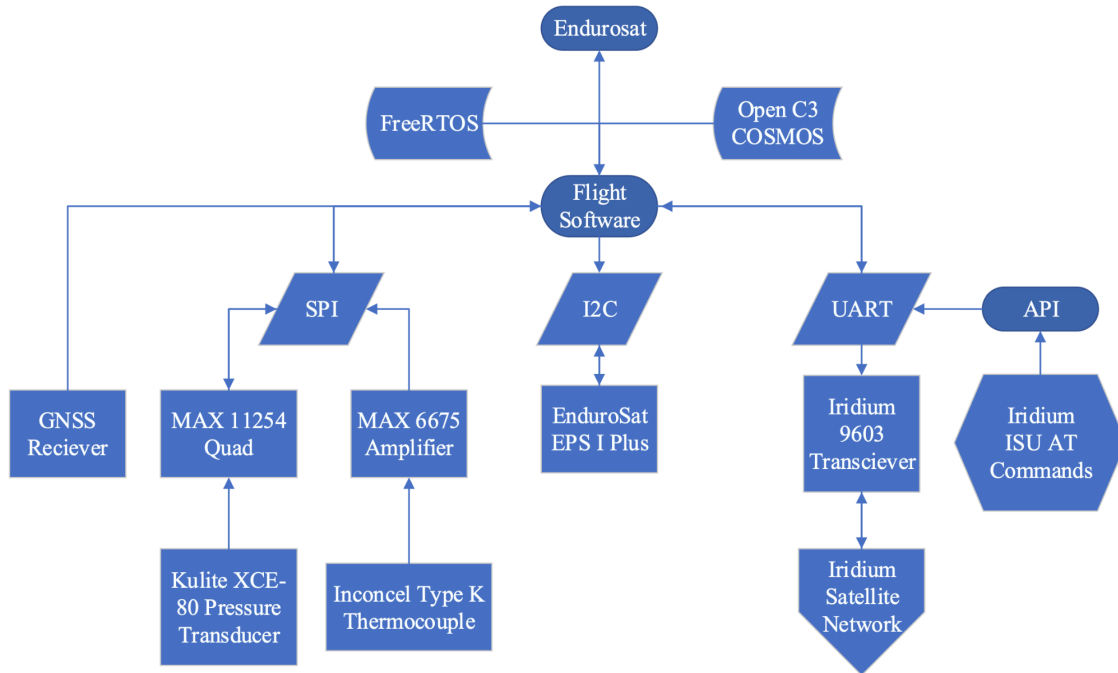
Figure 12: Data Distribution Flowchart

Communications

The communications team is tasked with transferring data off HEDGE during the orbital phase and difficult re-entry regime of flight. The components involved with the communications subsystem include the RockBLOCK 9603 Transceiver, which is an Iridium 9603 transceiver that is already mounted to a board for easy testing and development and the 2J Antennas 2JP0133BGFz As mentioned above, as part of their capstone, electrical engineering students completed two circuit boards, one being the avionics board and the other being the Iridium transceiver board. It was realized during testing that the Iridium board lacked the required power conditioning circuitry to send signals. To get around this, it was decided that a RockBLOCK would be used on board HEDGE as it already has the necessary power conditioning circuitry built in and thus would result in a shorter design cycle. The 2JP0133BGFz combines an Iridium and GNSS antenna into one small board with pre-soldered connectors, reducing the complexity during integration. The Iridium antenna on the 2JP0133BGFz is used for communication between the RockBLOCK 9603, onboard HEDGE, and the Iridium communications network that will transmit the data to the ground. The 2J board also has a GNSS receiver that is compatible with both GPS and GLONASS.

During this past semester the communications team activated and tested a RockBLOCK 9603. Once this activation was completed, the hardware was turned over to the software and avionics team to continue integrating communication hardware into the system. The communications team also acquired two additional RockBLOCKs to allow both the Software and Avionics team and communications team to conduct testing at the same time.

18

There are some main goals of the communication team that we strived to achieve this year. We wanted HEDGE to be able to transmit data to an Iridium and then back down to a Ground Station. We wanted that data to be automatically collected, independent of user request. Then, upon re-entry, HEDGE shall collect four temperature and four pressure measurements and one GNSS position every six seconds (send seven sets every forty seconds). However, in orbit, HEDGE shall collect and send data every hour. We also wanted to make sure that our transceiver and antenna shall be compatible with the Iridium Constellation and along with that we need HEDGE to be compliant with FCC and federal regulations. We successfully achieved all of this except for the last point about complying with regulations. In order to do this, we must apply for a license to operate radios in space. This application opens during the summer and we cannot do it at this time during the semester.

Subsystem Level Constraints

The concept of operations of HEDGE makes it infeasible to use ground stations directly. Therefore, to transfer data off the spacecraft during re-entry, we must direct the data back into space to a relay satellite that can transmit the data to the ground. This method was recently proven by SpaceX's IFT-3 in which they were able to relay data and video back to Starlink satellites and transmit it to the ground in real time (*Starship's Third Flight Test*, 2023). HEDGE will be different as the data transmission rate is much lower consisting of packets of collected data as opposed to live video. One difficulty specific to HEDGE when compared to SpaceX's Starship is that HEDGE is that the link margin may be smaller. Students who have worked on HEDGE in previous years have performed detailed analysis to assess the different options, such as Iridium or Globalstar, for relay satellite providers and chose Iridium. This year, the team agreed with their assessment, but we would recommend further study into other networks for future generations of HEDGE, should they be funded, such as Starlink once IoT (Internet of Things) options are developed. This may allow for an increase in coverage while our CubeSat is in orbit and would provide a more reliable connection.

The 2J 2JP0133BGFz dual antenna is our main connection between the Iridium satellite system and HEDGE in ensuring a successful flight. We had two options on where to place the antenna. We chose to put the antenna near the electronics on the back of our cubesat as seen in Fig. 9. This area is more safely tucked away in between the deployed fins. If both are to be attached to the fins of HEDGE, a concern is heat exposure. During re-entry, there are concerns that the heat will melt and destroy the antenna and transceiver quickly which would provide us with insufficient data to report back on the status of HEDGE. To combat this, we can put the antenna on the back plate of the main cubesat body. This will be the coolest place for the antenna. Additionally, re-entry causes a formation of plasma sheath that surrounds the CubeSat which could possibly interfere with the signal behavior and prohibit correct data. Our signal should be able to pass through. A way to solve this problem is to have the antenna be more pointed towards the Iridium satellite during re-entry as to minimize the amount of plasma sheath that we have to

go through, as the sheath is a cone shape around the cubesat and is more open at the opposite side of the leading edge of the cubesat. We conducted tests using aluminum foil and the antenna and transceiver to test the strength of the antenna at different angles using the position of the Iridium satellites. The test was done to see how well the antenna was able to transmit signals through a metal plate. Inconel was not available at the time of testing and aluminum foil was wrapped around the antenna in a shape that resembles the deployed fins of the cubesat. This allows us to see how likely we are to have successful transmissions while we are re-entering the atmosphere. The results of these tests are summarized below.

Components and Justification

Our team selected the use of the RockBLOCK 9603 transceiver based on previous year's analysis and flight heritage. It also boasts a low power draw with an idle consumption of 195 mA and 1.5 A during peak transmit in a small, light form factor.

For the GPS and Iridium antennas we chose the 2JP0133BGF Iridium Certified Antenna. The 2J antenna is a combination of an Iridium and GPS antenna mounted on a ground plane. It is lightweight, cost effective and power efficient. Connectors are preinstalled to reduce integration and complexity. It is also ground plane independent meaning it is already mounted to a ground plane. The 2J operates from -40 degrees celsius to 85 degrees celsius. Re-entry has the ability to reach over 1,000 degrees celsius. This causes quite a concern for damaging our transmitter before we can send any data up to the satellite from our CubeSat. In order to give our antennas the best chance of survival we need to place the antenna inside the enclosure of the Inconel fins which can again be seen in Figure 7. This makes it safer, but leads to a concern of how well the signal is able to penetrate the Inconel metal.

Prototyping and Analysis

In order to test the validity of using the transceiver while within the confines of the fins, we have designed an experiment to test the signal strength while transmitting a signal with aluminum plates on all sides of the antenna, as seen in Figure 13. First we produced a CAD drawing of an assembly that would hold our test plates. The stand was 3D printed and has the same dimensions as the CubeSat. The aluminum sheets were held just like how they would be while the fins are deployed and the cubesat is gliding through the atmosphere.
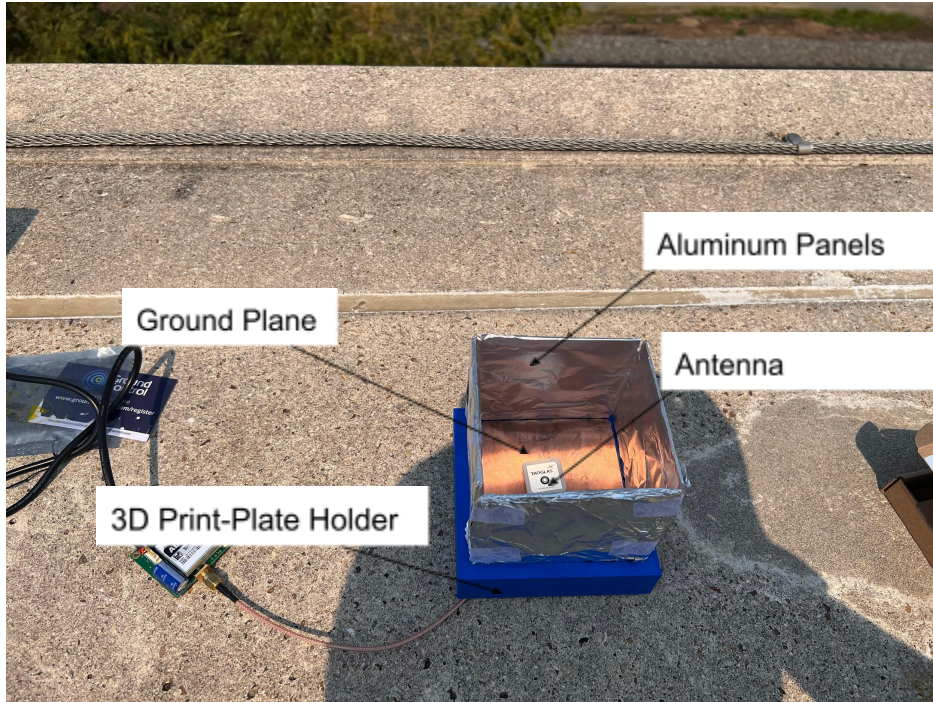
Figure 13: Experimental Antenna Setup

The stand has a hollow bottom which allows for a copper ground plane to run underneath with our transceiver attached to it. The copper ground plane is needed for the antenna to sit on while it is in use. It helps make a more effective radiation pattern with the antenna's signal. In some cases the ground plane helps reflect the signal from downwards to upwards. We then took our design set up outside and set the stand up at different angles to a Iridium Satellite passing overhead. We used an online tracker to see exactly where the satellite was and saw how much of an angle that created with our experimental set up. We then sent a test signal to see if it went through. The angle was calculated from the vertical axis that runs straight up from the antenna. With zero degrees being pointed in the same direction as the antenna.

Table 5: Angle Transmission Test

Angle With Iridium Satellite	Successful Attempts	Total Tests
30 degrees	1	1
45 degrees	2	2
60 degrees	1	3
75 degrees	0	3
90 degrees	0	3

We also covered the antenna in aluminum and saw if the signal can be sent through it completely. This information informed us of what angles the transceiver is able to send messages. When the CubeSat is re-entering, it may be at angles where the fins completely cover the signal path to the Iridium satellite. From our experimental data, we can see that our signal becomes unsuccessful at an angle of 60 degrees from an axis that goes straight up from our antenna, perpendicular to the ground plane that the antenna is attached to.

From our data and our expected orientation of the CubeSat, it was decided that we do not need to place the antenna higher from the bottom of the fin. We can leave it lower because our tests showed that the antenna was able to transmit at around 45 degrees when it was as low as it could go. We moved the ground plan up a few centimeters and it still did not work with 60 degrees. There also comes the concern of heat that comes in from around the fins and the fact that the heat shield

Orbit and Iridium Satellite Coverage

When in search of potential launch vehicles to launch HEDGE, it is important to consider launch parameters that will help meet our mission objective. Different orbit inclinations will give us different times under coverage of the Iridium Satellites. To determine which inclinations had the most Iridium Constellation coverage, we first uploaded an accurate Iridium Satellite Constellation onto ANSYS STK. The constellation is set up with 6 planes and 11 satellites per plane. Then we defined multiple satellites with a 200 km altitude and with inclinations of 30, 45, 60, 75, and 90 degrees on ANSYS System Tool Kit (STK). To account for potential variations in relative positions upon the release of HEDGE in relation to the Iridium constellation, we conducted tests across inclinations corresponding to multiple right ascensions of the ascending node: 0, 90, 180, and 270 degrees. Thus, there were four satellites for each inclination. Then, using features on ANSYS STK helped to determine the time of physical presence under the iridium coverage zones in a 24-hour span. Figure 13 shows the average time under coverage for each inclination. The result indicates that a 90 degree orbit, also known as a polar orbit, would give HEDGE the best odds in being in communication with the Iridium constellation throughout its orbital lifetime and re-entry. It is important to note that this analysis doesn't consider the 60 degree reception angle, and it is only purposeful in indicating which orbit inclination gives HEDGE the most time under the Iridium coverage zones.
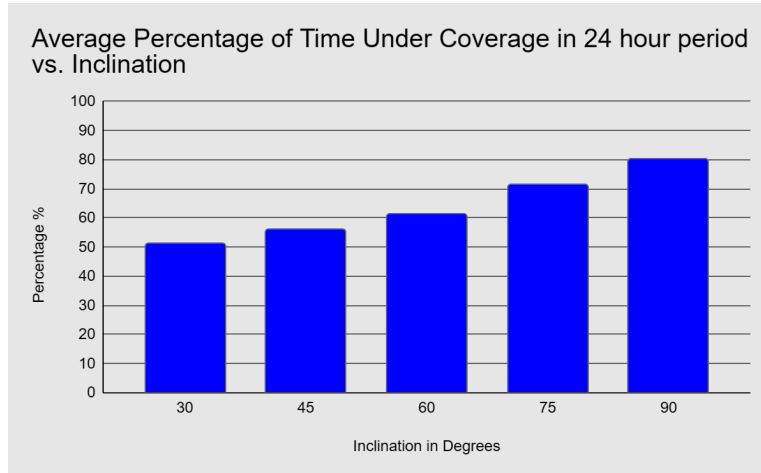
Figure 14: Average Time under coverage of satellites of different inclinations

Link Budget

During missions, data transmission faces risks of loss as it travels between the transmitter and the receiver. It is crucial to predict and track these losses and gains to accurately assess the reliability and efficiency of the communication link. By estimating a link budget, mission staff can make informed decisions regarding the optimization and improvement of their data transmission systems, ensuring optimal performance in all scenarios. The use of a link budget enables the quantification of the link performance through a calculator that assesses whether a communications link will operate successfully. This calculation takes into account the gains and losses at each stage of the transmission path from the transmitter to the receiver. By taking into account the transmitter power, the loss of signal strength due to propagation, the antenna gains, the feedline losses, and the amplifications of the signal, the link budget will calculate the power of the receiver given by the output power of the transmitter. The use of a link budget is crucial for designing and analyzing performance of communication systems ("What Is a Link Budget", n.d.).

A simple link budget was created through the utilization of Ansys Systems Tool Kit (STK). STK offers a physics-based modeling environment, enabling the analysis of space platforms and payloads within a dynamic and realistic three-dimensional simulation. With its capability to simulate the entire system-of-systems operation, at any given location and time, STK provides insights into the behavior and mission performance, offering a comprehensive understanding of the system's dynamics. ("Ansys STK", n.d.) To get the link budget, a new scenario was created in STK with the Iridium satellite and the HEDGE satellite added into the object browser. Next, a transmitter was modeled on the HEDGE satellite using a Gaussian model, a specific mathematical expression that is used to model the capabilities of the link. The model has a design frequency of 1.621 GHz, chosen from the 1.616-1.627 GHz frequency range of the RockBlock 9603 Transceiver, and a half beam angle of 60 degrees (See Figure 14 for calculation of the half beam angle). After that a sensor was attached to the Iridium satellite that will be targeted towards the HEDGE satellite. The sensor selected was a half conic with a 62.3

degree cone half angle. Next a receiver was modeled with a Gaussian antenna on the sensor that has the same parameters as the transmitter with a design frequency of 1.621 GHz and a half beam angle of 62.3 degrees. After all those steps were completed, the Iridium constellation was set up by adding in 6 planes of 11 satellites per plane to account for the 66 low earth orbiting satellites. With both HEDGE and Iridium satellites set up, we have a clear visual of what the low earth orbiting satellites look like with the color green showing the transmitter's potential paths and blue showing the receiver's potential paths (See Figure 15). The link budget was then calculated by observing when the receiver of the iridium satellites and the transmitter of the HEDGE satellite were linked. There were two different simulations that were done. One simulation had a transmitter with 60 degree half beam angle (as mentioned above) and another had a 90 degree half beam angle, so we could determine which simulation has the better connection to Iridium. The results showed that a 90 degree half beam angle is best. As the simulation gets more detailed, future tests are going to be needed to determine how we can get that coverage.
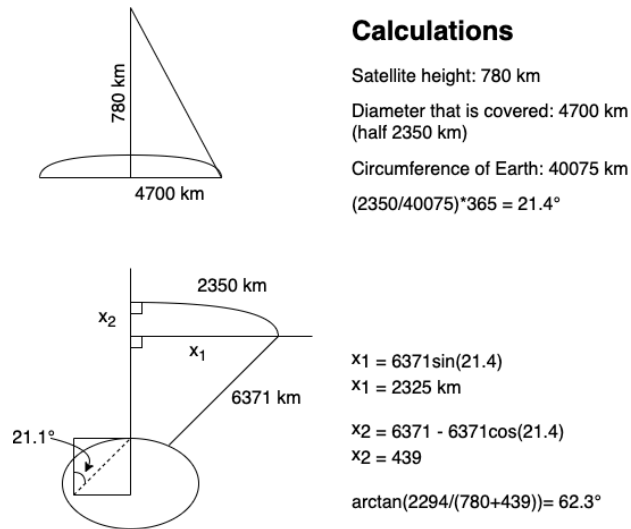

Calculations

Satellite height: 780 km

Diameter that is covered: 4700 km (half 2350 km)

Circumference of Earth: 40075 km

$(2350/40075)*365 = 21.4°$

$x1 = 6371\sin(21.4)$
$x1 = 2325$ km

$x2 = 6371 - 6371\cos(21.4)$
$x2 = 439$

$\arctan(2294/(780+439)) = 62.3°$

Figure 15: Calculations for the half beam angle

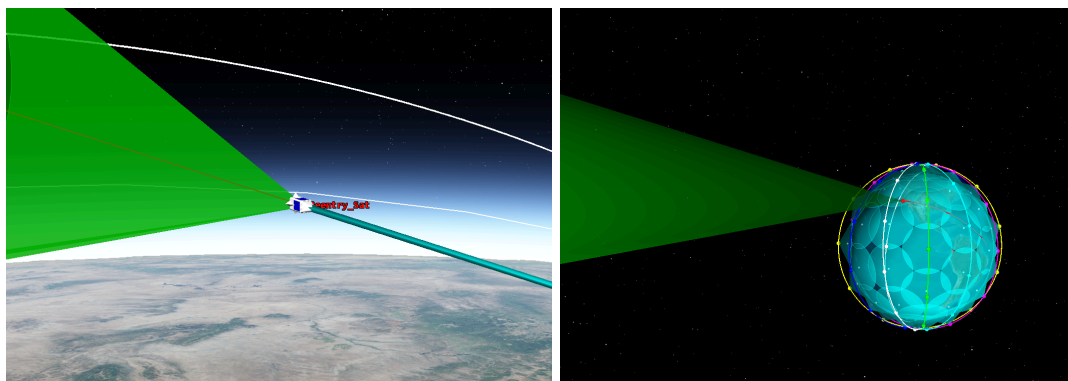
Figure 16: STK model of HEDGE and Iridium

Attitude Determination and Control Systems (ADACS) & Orbits

Subsystem Level Constraints

The Attitude Determination and Control Systems (ADACS) and Orbits subsystem works in accordance with four primary requirements. First, promoting and optimizing highly stable flight upon reentry. Testing the feasibility of CubeSat technology intended for hypersonic research mandates that stable flight be maintained. After tumbling in low-earth orbit (LEO), the craft in theory will orient itself as atmospheric density increases and produce data until it's burn-up point is reached. Without active controls, HEDGE relies on the aerodynamic design to produce stability. This is quantified through the static margin, a measure of the location difference between the centers of both mass (CoM) and pressure (CoP). The secondary requirement set by the Communications subsystem requires our CubeSat be in communication with the Iridium satellite constellation. The launch must follow a trajectory within the existing satellite coverage, and antenna placement must allow for the craft to receive a mostly uninterrupted signal. HEDGE will accomplish this via a polar orbital flight path, which maximizes the amount of coverage the satellite will have. This was determined through orbital simulations and iridium satellite configuration analysis, which shows optimal coverage utilizing a polar orbit. The third subsystem requirement calls ADACS to limit component weight to ensure successful launch provider integration, and the final one constrains the volume of our subsystem components. All constraints, as well as the static margin, are subject to the design limitations regarding configuration and component mass set by the Structures and Integration subsystem. These apply to our subsystem by limiting the mass contribution to 100 grams and volume contribution to 40 cubic centimeters. The final condition is the minimization of the power consumed by ADACS components. The guidance of each subsystem requirement further accentuates the CubeSat's pre-existing demand for design simplicity, which are based upon volume restrictions and subteam component compatibility.

Components and Justification

Upon atmospheric re-entry, highly stable flight for HEDGE is achieved without using active control, or real-time orientation corrective commands. Instead, a number of passive methods were established to give the CubeSat the highest probability of successful attitude control within constraint guidelines. Relying on such methods minimizes power consumption, volume, weight, cost, and complexities of the subsystem. This is manifested through the implementation of an aerodynamically stable design. Aerodynamic stability is characterized as the craft's response to changes in the air in reaching balanced flight behavior, which can be quantified using the static margin. The static margin is a stability metric describing the distance between the center of gravity and center of pressure, or the neutral point. The ADACS team recommends a static margin of at least the length of one spacecraft diameter to establish aerodynamic stability. With a square body, the effective diameter of HEDGE, and the recommended static margin is the width, or 100 mm. Analysis from *Passive Stabilization Systems for CubeSat Nanosatellites: General Principles and Features* (Belokonov et al., 2019) recommends a smaller margin of 10-15% of the craft's characteristic length. This concept works by engaging the craft geometry so that it may orient itself correctly upon reentry. Locations of the center of pressure and center of mass are determined through computational fluid dynamics and structural analysis. Results are discussed below.

The physical elements of the ADACS design approach are present in the flush air data sensing system (FADS). The attitude determination is done with the FADS system which will measure the pressure behind the shockwave that HEDGE will experience as it re-enters on each side of the craft's nose. The analog pressure measurements will be converted to a digital signal and sent to the flight computer of HEDGE. The OBC will use the algorithms to convert the digital pressure measurements into angle of attack and angle of sideslip measurements showing the stability of the craft at a point in time. While aerodynamic stability should ensure the craft rights itself when it re-enters the FADS system will determine if the aerodynamic stability was successful in doing so.

The aforementioned system will be constructed to withstand the high temperature conditions experienced upon reentry. Four one millimeter pressure tap holes will be bored in the craft, one on each face of the nose cone, flush to the exterior wall and through to the interior, allowing pressure to be measured. 3/32" outer diameter (OD) McMaster-Carr 316 Stainless Steel tubing will be connected to the interior side of the hole. At 0.58 grams per inch, this tubing will allow us to stay within our mass budget. The thermal insulation provided by the structure of the craft will ensure temperatures do not exceed the 1,088 K maximum of the steel. Cole-Parmer IDEX Ethylene-Tetrafluoroethylene (ETFE) tubing will be fitted to the end of the steel tubes with a matching 3/32" ID, at 0.17 grams per inch. This material has a maximum operating temperature of 353K so it is necessary for the steel portion of the apparatus to be long enough to allow the flow to cool substantially. A McMaster-Carr Compression Spring will be used to hold the tubing together. Four Kulite XCE-080 miniature pressure transducers will record the data obtained from flow outside the craft. They will be located near the center of the craft, at the end of the flexible ETFE tubing. Based on the resolution of the onboard ADC, minimum pressure changes of 2.6 Pa will be detected during flight, allowing for a measure of attitude change. The four pressure sensors, 16.44 inches of steel tubing, 3.64 inches of ETFE tubing, and roughly 0.84 inches of spring will contribute approximately 14.3 grams of mass to the spacecraft. It will also have a volume contribution approximately 13 cubic centimeters, which are both within our subsystem limits.

The post-flight analysis will evaluate the stability of HEDGE during reentry via its attitude as a function of time. HEDGE's attitude will be estimated using pressure data from taps on each side of the nose. The OBC will report the pressure data, as well as position data from the GNSS. After the flight, an attitude determination algorithm will be used to generate a plot of attitude over the course of the flight.

Prototyping and Analysis

The attitude determination algorithm (see Appendix G) assumes 2-dimensional compressible flow around a wedge. For low angles of attack (see Figure 17, middle diagram), we expect oblique shocks to form on both sides of the craft. At sufficiently large angles of attack (greater than 14.12°, the half-wedge angle of HEDGE's nose), we expect an oblique shock to form on the windward side of the craft and an expansion fan to form on the lee side (see Figure 17, right diagram). The velocity of HEDGE (and thereby its flight Mach number) is evaluated as the rate of change of position of the craft, while the ambient pressure and temperature are assumed to be a function of altitude (based on the ISO's International Standard Atmosphere).
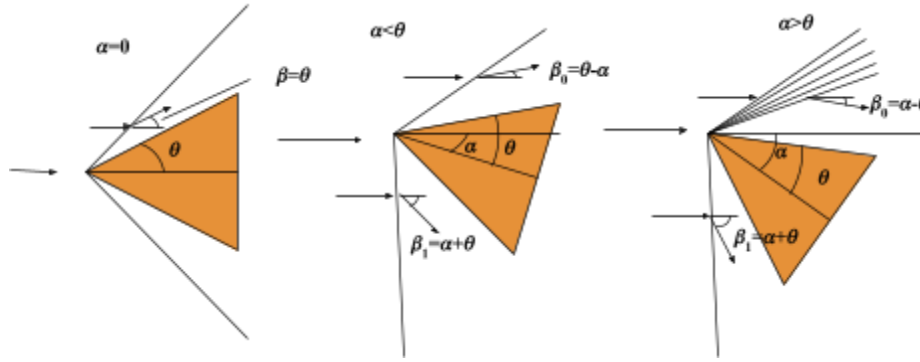
26

Figure 17: 2-D shock formations around HEDGE's nose cone

α is angle of attack, θ is half-wedge angle ($\approx 14.12°$), βs are the deflection angles of the flow on either side of HEDGE

The algorithm takes the ratio of static pressure along the surface of HEDGE's nose cone (P_1, recorded by the pressure transducers) to the ambient static pressure (P_0) as an input. A pressure ratio (P_1/P_0) less than one indicates the presence of a Prandtl-Meyer expansion fan. If the pressure ratio is greater than one, that side of the craft is experiencing an oblique shock. The resulting profile of angle of attack computed from the pressure ratio is shown in Figure 18.
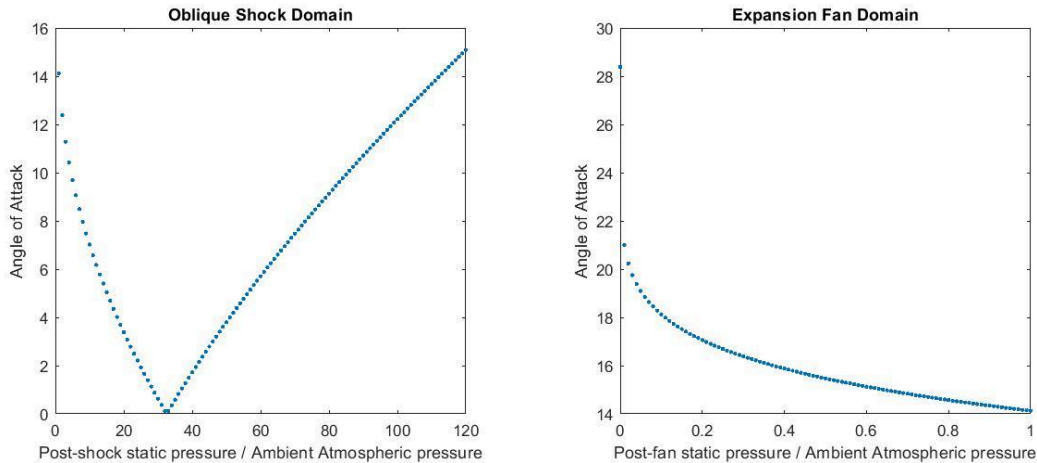

Figure 18: angle of attack (α) as a function of pressure ratio (P_1/P_0)

It is important to note that while each pressure transducer's data is sufficient to calculate angle of attack, transducers on opposing sides of HEDGE measure the same angle of attack, meaning that they can 'disagree.' Detecting disagreement on HEDGE's angle of attack will suggest that there is some kind of malfunction occurring.

Orbital Lifetime

The objective of using the ANSYS STK software was to predict and analyze specific orbital properties of HEDGE. More specifically, through the use of the orbital lifetime features in the software, we predicted an orbital lifetime of HEDGE. However, throughout this analysis, assumptions about the properties of HEDGE had to be made which are explained in the following paragraphs.

ANSYS STK has a built-in tool that predicts the lifetime of satellites. It first requires inserting a satellite by defining properties such as altitude and eccentricity. Figure 18 shows the plug-in feature of the life time calculator. Following mission constraints, a satellite with a circular orbit of 200 km was created in ANSYS STK so that we can use the lifetime plug-in for HEDGE.

Because of our mission constraints, we can assume an initial altitude of 200 km and a mass of 5.92938kg. With the help of the Structures sub-team, we concluded the drag area to be 0.019 square meters. This is the area of the face that is normal to the trajectory of HEDGE. When experimenting with the lifetime tool, the area exposed to the sun has no effect on the lifetime of the orbit, especially when dealing with satellites as small as HEDGE. Thus, the area exposed to the sun was estimated to be 0.07 square meters which is assumed to be half the surface area of a standard 3U Cubesat. The coefficient of drag for a 3U cubesat is 2.2 (Prado, 2018). The solar radiation pressure for cubesat satellites is found to be insignificant (McInnes, 2011). Therefore, for our simulation, we simply assumed a cr of 1. This means the HEDGE would be perfectly absorbing. The propagator for the initial state tool used for the lifetime calculation was J4Pertubation. The initial orbit was also chosen to be circular since we cannot determine specific release conditions. Table 5 below shows the assumptions that were used for HEDGE for the plug in.

Table 5: Assumptions of HEDGE for plug in

Propagator	J4Pertubation
Altitude	200 km
Inclination	90°
Eccentricity	0
Drag Coefficient (C_d)	2.2 (Prado, 2018)
Solar Radiation Pressure Coefficient (C_r)	1
Drag Area	0.019 m^2
Area Exposed to Sun	0.07 m^2
Mass	5.92938 kg

Lifetime (Result): 95 orbits : 5 days. The simulation predicts a 5 day orbital lifetime which achieves the current mission objectives.

Fluid Analysis

The computational fluid dynamics (CFD) simulations were used to determine stability parameters of the spacecraft reentry, specifically at the time when the orbit comes to an end and atmospheric reentry begins. This was conducted in collaboration with the Power, Thermal, Environment (PTE) subteam. For this simulation, reentry is assumed to start at an altitude of 80 km for which the ambient conditions can be seen in Table 6. This CFD was performed in order to predict the flow around the spacecraft at an anticipated condition of Mach 20 (5.245 km/s). From this, we aim to determine the pressure distribution and drag properties, both of which will be the focus of this section.

Table 6: Ambient conditions at 80 km altitude (*Properties of Standard Atmosphere*, n.d.)

Density (ρ_f)	1.57005E-05 kg/m^3
Kinematic Viscosity (μ_f)	1.31682E-05 N-s/m^2
Temperature (T)	196.65 K
Pressure (P)	0.88628 Pa

ANSYS Fluent and ANSYS Workbench were utilized to conduct the CFD in accordance with industry standard software, student work, and professional guidance from Dr. Xinfeng Gao. Dr. Gao is a University of Virginia professor with a background and expertise in CFD, and generously offered her support as our subject matter expert (SME). For simplification of the initial analysis, the three dimensional model of HEDGE was reduced to a two dimensional body made up of simple geometric shapes shown in Figure 19. In addition, only half of the spacecraft was modeled for the CFD under the symmetry assumption allowing for faster computational times.
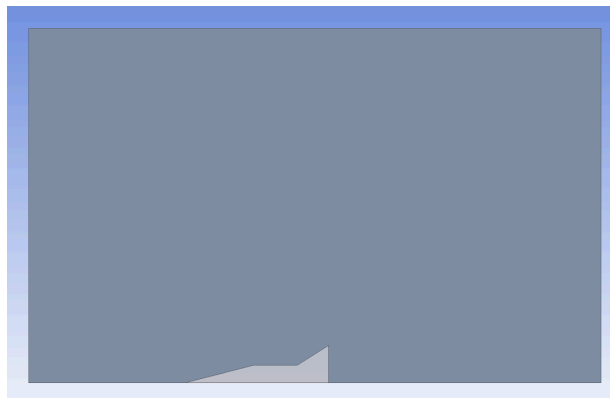

Figure 19: 2D CAD model of HEDGE used for the CFD simulation

The box that is drawn around the model represents the fluid domain where the simulation will take place and its size is dependent on the height w, a characteristic dimension to describe the spacecraft shown in Figure 19. Consulting with our subject matter expert yielded the following domain geometry: the top boundary of the domain is at a distance of 10w, the front boundary is at 3w, and the back boundary is at 6w. These distances were all predicted to make sure the simulation domain would be large enough to accurately capture the flow near the wall of the spacecraft, while also leaving some room for unhindered freestream flow far from the wall.

Figure 20: Zoomed in image of hedge showing "w" dimension

For the mesh, viscous effects were considered for which an accurate boundary layer (BL) depiction was required. To determine an initial prediction for the BL, Eqn. 1 and Eqn. 2 were used along with input from a subject matter expert. Eqn. 1 is the formula for y+, a dimensionless length characteristic used to describe the size of the boundary layer, based on fluid density (ρ_f), fluid viscosity (μ_f), friction velocity (u_τ), and the first cell height (y_p). Eqn. 2 is used to calculate the friction velocity based on the wall shear stress (τ_{wall}) and the fluid density. The density and viscosity used in the are listed in Table 5 and our subject matter expert advised us with estimates for the wall shear stress (τ_{wall} = 800 Pa) and the dimensionless characteristic boundary layer parameter (y^+ = 18), both of which are based on their experience in hypersonic simulations. From this, the cell height for the first layer of cells (y_p) from the wall was determined to be approximately 2.11 mm. This cell height was used to depict the boundary layer with two layers of structured mesh directly above the wall shown in Figure 21. Beyond this structured area, a default triangle based mesh is used along with an inflation parameter of 1.2 that gradually increases the size of the cells farther from the spacecraft wall by that factor.

$$y^+ = \frac{\rho_f u_\tau y_p}{\mu_f} \qquad\qquad \text{Eqn. 1}$$

$$u_\tau = \sqrt{\frac{\tau_{wall}}{\rho_f}} \qquad\qquad \text{Eqn. 2}$$

In order to decide on mesh size, our subject matter expert advised us to simplify mesh generation by changing the number of wall divisions along the 2D model of our spacecraft shown in Figure 19. To conduct a grid convergence study, four different meshes were generated where the number of wall divisions on each wall was changed for every iteration. The four walls of the spacecraft are labeled in Figure 22. In order to simplify the generation of the initial mesh, the number of divisions on the walls was set equal to the number of length of the wall, in terms of millimeters. For example, wall surface 2 has a length of ~185 mm, so the number of wall divisions was set to 185 and a similar approach was used for the rest of the walls. To refine the mesh, we were advised to proportionally increase the number of divisions on each wall, so the refined meshes had 2x, 3x, and 4x the millimeter length of the respective wall. Finally, the 4x mesh was used for the results attained in this simulation and had a size of 57,238 elements.
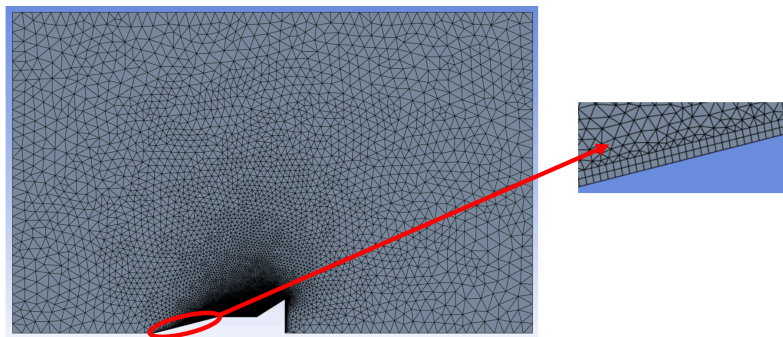

Figure 21: Initial generated mesh and near wall representation of boundary layer

In order to verify the validity of the mesh, a grid convergence study was conducted by analyzing the static pressure along the walls of the spacecraft body. Specifically, we looked at the static pressure readings given by the CFD at the onset of the Prandtl-Meyer expansion fan which occurs at the vertex between edges A and B shown in Figure 22. This point was chosen as the section of analysis because the expansion fan develops a little bit of time after the flow interacts with the spacecraft allowing the flow to have some time to develop. This effect can also be seen in the bottom image of Figure 24 where that region has a flight blue to green gradient. As seen in Figure 23, the static pressure at that expansion fan was plotted for each mesh iteration. Between the first and second iteration, which represent the 1x and 2x meshes respectively, there seems to be a large variation. However, this variation significantly decreases between the 3x and 4x meshes, shown by mesh iteration 3 and 4, so this was used as evidence to justify the 4x mesh as the best option for this simulation.
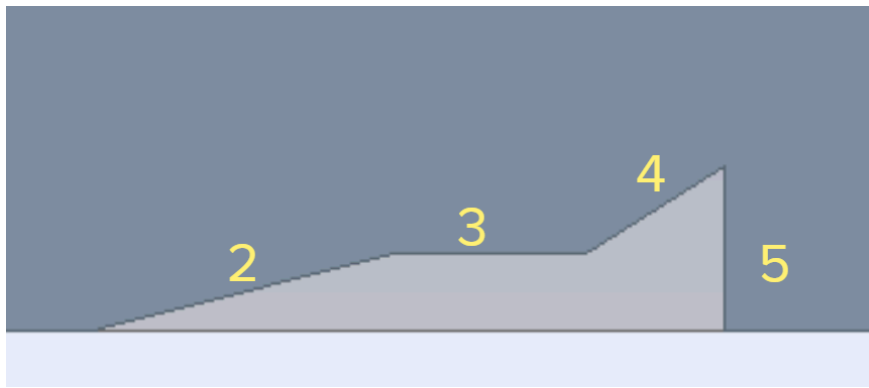

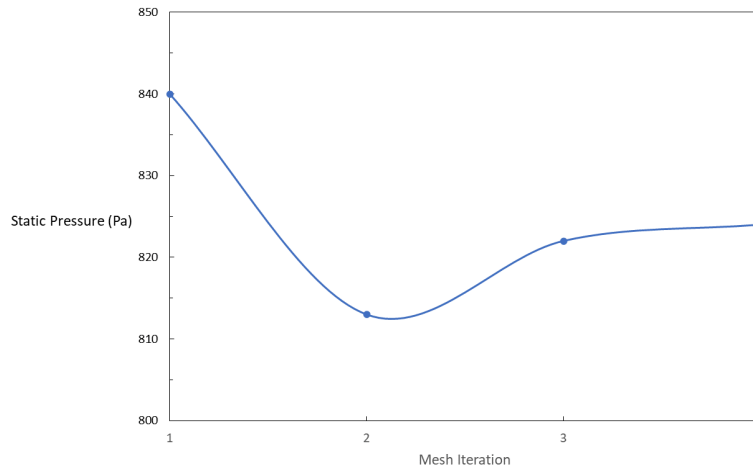Figure 22: Labeled walls of HEDGE body

Figure 23: Static pressure at the expansion fan

Boundary conditions were based on basic simplifying assumptions and are supported by guidance by a subject matter expert. The properties shown in Table 5 reflect the ambient air conditions used to define the fluid domain, and these are present in the boundary condition

settings. A gauge pressure of 0 Pa was applied to the 'Outlet' wall on the right of the mesh, allowing the simulation to solve Navier-Stokes equations in evaluating pressure at various locations. A gauge pressure of zero represents zero pressure additional to the ambient pressure at altitude. No-slip conditions were applied to the surface of the Cubesat's 'body', allowing for the creation of a boundary layer in the results. Top and bottom domain walls were also given a zero-shear condition to portray an accurate and open fluid domain.

Results

The simulation ran through 800 iterations, a choice guided by a subject matter expert and typical iterative ranges for crafts of this size and complexity. Our findings report an observed drag coefficient of 0.0432. Given the smaller surface area of HEDGE, the drag coefficient is relatively small in comparison with typical ranges for larger spacecraft or small aircrafts. With this number, further evaluations of the flight characteristics the Cubesat may exhibit are now possible. HEDGE's symmetry is implemented into the mesh design, meaning that simulations assume the center of pressure is located along the craft's axis of symmetry.

Pictured below are the contours for mach number and static pressure produced. In the top photo, the previously discussed boundary layer is shown, with the presence of an expansion fan represented in the top picture of figure 24, through the larger blue area touching the back fins of HEDGE.
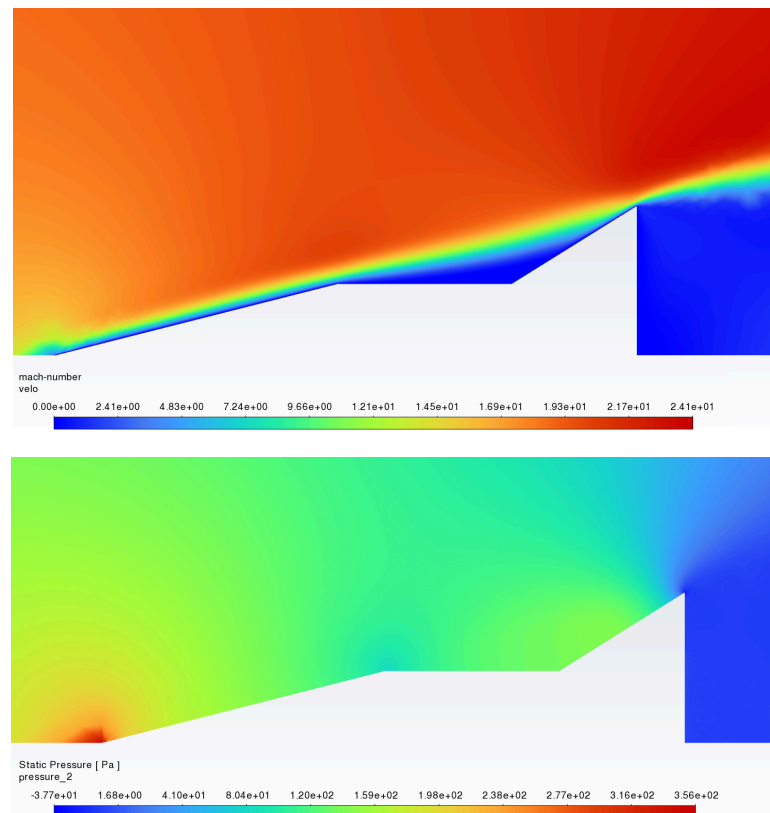

Figure 24: Contours of Mach Number (Top) and Static Pressure (Bottom)

The location of the center of pressure of the aircraft was found to be 176.8 mm from the tip of the nose cone. Using the Solidworks Evaluation Tool, we found the final center of mass to

32

be 199.52 mm from the tip of the nose cone. This results in an estimated static margin of -22.72 mm, meaning that the center of pressure is located behind the center of mass.

It should be noted that simplifications in both boundary conditions and the geometry of the 2D model contribute to the reduction of the static margin. Previously conducted analytical calculations (by last year's design class) place the center of pressure further aft. Using compressible flow equations modeling expansion fan and shockwaves, with angles of attack of 5° and 15°, centers of pressure were found to be 289.3 mm and 299.1 mm, respectively. This results in a static margin of +89.78 mm and +99.58 mm, respectively. This does not meet the above requirement of a static margin of at least 100 mm but it does meet the requirement of 10-15% of length. In future work, a 3D CFD model is recommended to more accurately estimate the center of pressure.

Power, Thermal and Environment

Subsystem Level

The Power, Thermal, and Environment (PTE) subsystem is bounded by seven design requirements that will ensure a successful mission. At a subsystem level, all equipment, including power sources, shielding, and wiring, must conform to cubesat standards. All equipment and large debris must deteriorate, after the test window, under aerodynamic and thermal stresses during reentry. Analyzing "sub-subsystems" individually, no materials used in HEDGE should outgas or deteriorate under space conditions prior to reentry, and no thermal shielding materials may survive fluctuating high and low temperatures. However, to achieve communication goals, the thermal constraints of electronics, materials, and structures must not be exceeded during reentry temperature phases. The battery and electrical power system must supply sufficient voltage and current to all electronic subsystems according to a power schedule. The battery life must survive the mission of approximately 16 days while being recharged by solar panels, and the battery must maintain charge throughout pre-launch standby time.

Power Consumption by Mission Phase

The power system must be capable of supplying enough power for all other systems within HEDGE to function properly for the entire duration of the mission. There are three stages of the mission which are relevant for calculating the power budget. The first stage is the pre-launch phase, where the Cubesat is stored at the facility while waiting for the launch date. The length of this stage is estimated to be between one and six months. During this time, charged batteries present within HEDGE are anticipated to lose around 3% of the initial charge per month, which still allows for the mission objectives to be met. The second stage is the orbit phase, which is when HEDGE resides in LEO while waiting to re-enter the atmosphere. This stage is anticipated to last no more than 16 days. During this stage, the average power consumption is low due to most components remaining dormant with the exception of hourly transmissions of positional data. The final stage is the re-entry phase, which has been estimated to last one hour in order to provide a large margin of error. During this phase, all systems will be operating at their maximum power consumption as data is collected and transmitted. Therefore, it is imperative that enough power is available after the first two stages to ensure full functionality of data collection.

Components and Justification: Power

    The power subsystem is composed of many individual elements, including an electrical power system (EPS), solar panels, charge controller, and auxiliary battery pack. The EPS is the EnduroSat EPS 1 Plus, which contains two internal batteries with a combined capacity of 20.8 watt hours. The EPS regulates power being supplied by the solar panels and battery pack, then distributes it to the remaining subsystems at the correct voltages while providing overcurrent protection. The solar panels are Endurosat 1U panels, four of which are mounted to the exterior of HEDGE. Each solar panel is capable of generating 2.4W under direct sunlight. The auxiliary battery pack is composed of four Samsung 35E 18650 3500 mAh lithium-ion battery cells wired in parallel and shrinkwrapped. A specialized mounting case was designed on SolidWorks that will secure the battery pack and charge controller to the interior of the nose cone. The purpose of the auxiliary battery is to ensure that the EPS internal batteries are fully charged when the re-entry begins. The auxiliary battery pack has a total capacity of 51.8 Wh, a voltage between 3.6 and 4.2V, and a maximum continuous discharge rate of 32A. The capacity of the battery was selected to be the largest possible given physical size constraints within the nose cone. Maximizing the battery's capacity provides the largest margin of error in the case that the solar panels generate less power than predicted. Finally an Adafruit bq24074 charge controller rated for 1.5A and 3.7-4.4V is secured to the side of the mounting case and wired between the auxiliary battery pack and EPS USB-SCIC port to ensure safe discharge and recharge of the lithium-ion batteries.

Prototyping and Analysis: Power

    Each component of the power subsystem is wired to other subsystems via buses of differing voltages to satisfy their power requirements. A diagram of how the power subsystem interfaces with the rest of HEDGE can be seen in figure 25. As seen in figure 25, all generated power flows into the EPS and is then rerouted to its designated destination. When exposed to sunlight, the solar panels produce power which flows past the maximum power point tracking (MPPT) and into the EPS. The MPPT is built into the solar panels and ensures that despite the varying charge produced, the battery is always charged at the appropriate voltage. When HEDGE is not exposed to sunlight, the EPS will draw power from its internal battery packs and the auxiliary battery pack. When in sunlight, HEDGE will power its subsystems using the current generated by the solar panels while using the excess current to recharge the batteries. This ensures that HEDGE always has a source of power available during all phases of orbit. From the EPS, power is routed through two buses: a 3.3V bus and a 5V bus. Power routed through the 3.3V bus is sent to the on-board computer (OBC). From the OBC, power is sent through analog to digital converters (ADC) and to the thermocouples and pressure transducers. Due to pressure transducer voltage requirements, it will be necessary to have a 10V bus to the custom electrical board interfacing with the pressure transducers. The Iridium transceiver has power supplied directly from the EPS via the 5V bus which can supply up to 4A of current and is therefore sufficient to support the maximum transmission current of 2.25A.
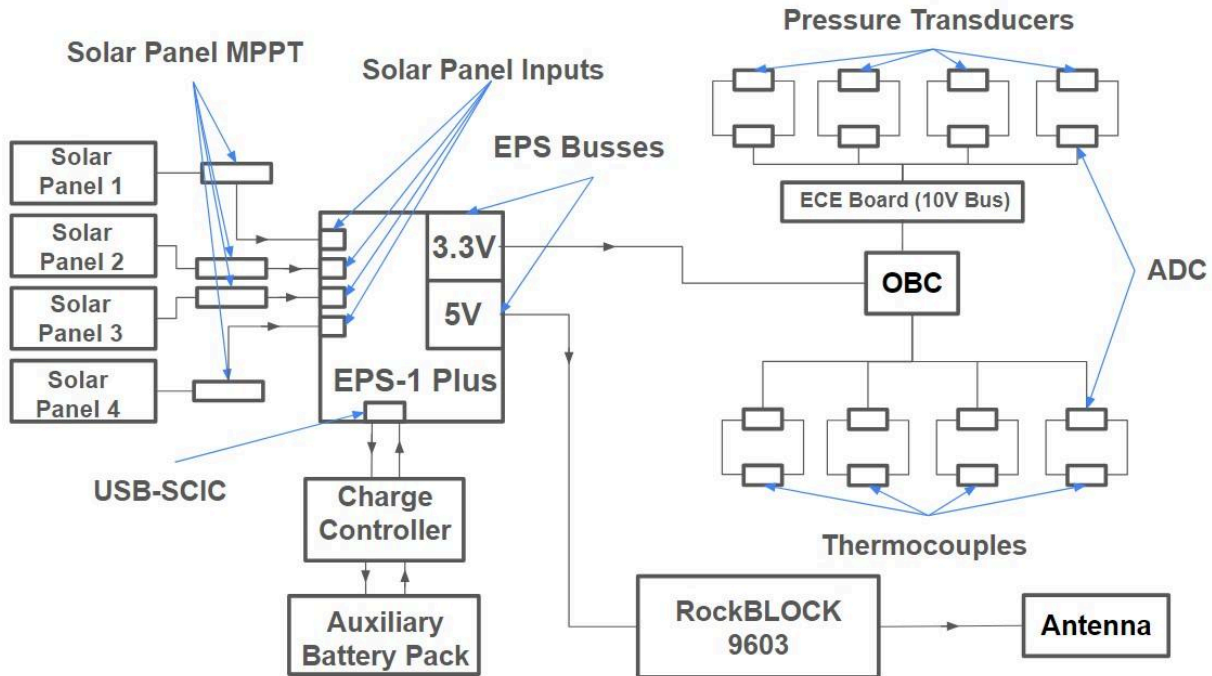
Figure 25: Power Diagram

The power budget (Appendix D) was calculated by determining the power consumption and generation of each mission phase to ensure power requirements could always be met. The predicted maximum power draw (MPD) during the re-entry phase is estimated to be 1.951 Wh (Figure 25). As previously stated, this is when all systems will be operating at their maximum power consumption for at most 1 hour. During orbit, the power draw will vary based on the duration of time the GNSS is activated on the OBC. The MPD will range from 179.58 to 651.98 Wh. The total power available for the mission is 543.9 Wh (Figure 25) which includes the power generated from the solar panels, the EPS battery, and the auxiliary battery accounting for dormant battery drainage on the latter two. This means that if the GNSS is activated for the entire mission, there will not be enough power supplied to the system.

There are three possible solutions to this problem. The first solution depends on the capabilities of the OBC. There is a pinout on the bus labeled EN GNSS which, in conjunction with a remote switch, could be used to turn the GNSS off when it isn't needed, conserving power for the reentry phase when the GNSS would be turned back on. At the moment, we are in communication with Endurosat to gain an understanding of this pinout's capabilities. The second option would be to add a custom GPS which can be turned on and off remotely and avoid using the OBC's GNSS entirely due to its large power consumption. The last solution would be to launch HEDGE from a sounding rocket (RockSat-X) which has a shorter mission duration, allowing the EPS battery, solar panels, and auxiliary battery pack to cover the entire power draw with the GNSS activated for the entire mission. If this were to happen, the longest possible mission duration while maintaining a factor of safety of at least 1.2 is 59.5 hours, or about 2.5 days. A breakdown of the power budget for a 2.5 day mission is located in Appendix D.

In order to calculate the power generated by the solar panels, the equation from the previous HEDGE thesis (2022-2023 Spacecraft Design Team) for the power generated in terms of axial angle (θ) and tilt angle (ϕ) was used. These values were then averaged for all angles

from 0 to 360 degrees to account for a random orientation to the sun at any point in time. The equation is as follows: $P = P_0 * |cos(\phi)| * (|cos(\theta)| + |cos(\theta + 90)|)$ where P_0 is the maximum power generation of one solar panel and P is the resulting power generation. It was assumed that HEDGE will spend one third of its total mission time in eclipse (2022-2023 Spacecraft Design Team), so the solar panels would only produce power two thirds of the time they are in orbit. The resulting total power generated by the solar panels is 497.7 Wh (Appendix D).

To summarize, during the period when HEDGE is waiting to launch, design requirements are met because no power is consumed and minimal power is lost as the batteries lie dormant. This dormant power loss was taken into account while developing the power budget and mission lifetime with a fully active GNSS. During the orbital phase, design requirements will be met if one of the three potential GNSS solutions is successfully implemented. This will ensure HEDGE has sufficient power during orbit while preserving enough for the re-entry phase. Design requirements for the re-entry phase will be met if sufficient battery charge remains after the orbital phase, which also relies on one of the GNSS solutions being implemented.

Components and Justification: Thermal

Thermal subsystem elements include a high temperature nose cone material and a material test panel. The nose cone of HEDGE, unlike other components, will be Zirconia coated Inconel 718. Inconel has significant flight heritage data and superior thermal and strength characteristics under mission conditions (2022-2023 Spacecraft Design Team). Material test panels will be provided by a project sponsor to test different TPS materials in flight. An initial material recommendation will be proposed based on a burn-up time analysis. Figure 26 shows a section diagram of HEDGE with the material test panels.
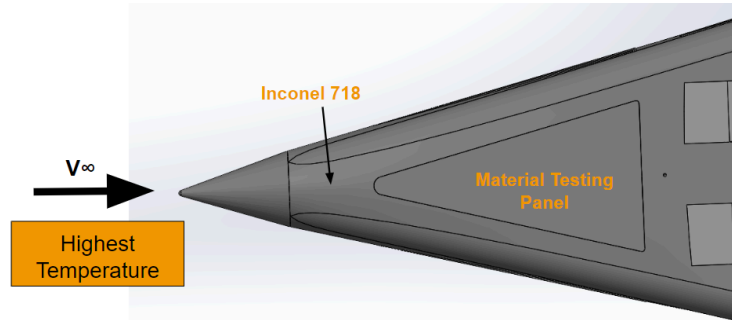

Figure 26: Inconel Placement on Nose of HEDGE

Estimated ablation times were calculated for PFA Teflon and Phenolic Nylon material testing panels, and estimated melting time was calculated for Inconel 718 material testing panels. PFA Teflon, Phenolic Nylon, and Inconel 718 were chosen due to their thermal characteristics and cost as well as the quantity of available data. Though ablative materials are uniquely suitable for dissipating heat, the ablation times of PFA Teflon and Phenolic Nylon are too low for HEDGE. Inconel 718, which withstands high temperatures but does not ablate, was therefore selected as an initial recommendation before panels are replaced by those from the project sponsor. In accordance with mission constraints, thermal protection system (TPS) materials must last long enough to support data transmission and eventually burn up alongside all other large debris.

Prototyping and Analysis: Thermal

     Analytical work relating to the thermal subsystem includes the calculation of heating rates for the most sensitive elements of HEDGE and the subsequent burn-up times for those elements during reentry. Prior to the completion of CFD and Finite Element Analysis (FEA), the aerodynamic model shown in Figure 7 was utilized for hand calculations.

     Figure 7 depicts the flow predicted by ADACS. The Virginia Tech Compressible Flow Calculator was used to find all pressures, temperatures, and Mach numbers, with an assumed initial Mach number of 20 at an altitude of 80 km (Appendix E-1). With an estimated wall temperature (Tw) of 1,000 °C across all regions, heating rates of 248.8 kW/m² across region 2 and 33.0 kW/m² across region 3 were calculated using Van Driest's theory of leading edge heat transfer for a laminar boundary layer (Appendix E-2). Van Driest's model, shown in Eqn. 3 was used, where adiabatic wall temperature, Taw, is equal to Eqn. 4 (White, 2022).

$$Q = Ch * (\rho e * Ue * Cpe * (Taw - Tw)) \qquad \text{Eqn. 3}$$

$$Te + r(\frac{Ue^2}{2Cpe}) \qquad \text{Eqn. 4}$$

     In Eqn. 3, Ch is a function of Reynolds Number that represents the local Stanton number, r is a function of Prandtl Number, and ρe, Ue, Te, and Cpe are post-shock density, velocity, temperature, and specific heat, respectively. At the tip of the nose cone in region 1, a heating rate of 4,464 kW/m² was found with the Fay-Riddell equation for Stagnation Point Heat Flux (Lee, Yang, and Kim, 2023). A summary of calculations can be found in Appendix E-3.

     Heating rates for each region were then used to calculate burn-up times and ablation times. The nose cone, which experiences the greatest thermal stress, will melt in 8.1 seconds, and Inconel testing panels would melt in approximately 25.9 seconds. Melt occurs when the structure reaches Inconel 718's melting point of 1610 K. Detailed calculations can be found in Appendix F. Under these conditions, HEDGE would have sufficient time to transmit data prior to complete burn-up. Ablation times were calculated using Hiester and Clark's report on standard evaluation for ablating materials. PFA Teflon has a mass loss rate of $0.0076*(Q)^{0.55}(P_{02})^{0.27}$, and Phenolic Nylon has a mass loss rate of $0.0017*(Q)^{0.56}(P_{02})^{0.13}$. Q is the heating rate in region 2 and P_{02} is the total pressure in region 2 (Hiester and Clark, 1966). PFA teflon panels would ablate in 0.122 seconds, while Phenolic-Nylon panels would ablate in 1.231 seconds (Appendix F). The ablation times are extremely short, so Inconel 718 is a superior material for the testing panels on HEDGE.

     Hand calculations were utilized to derive the boundary conditions for transient thermal/transient structural FEA in Ansys Mechanical. A simplified model of HEDGE was used for simulation, and the mesh is shown in Figure 28.
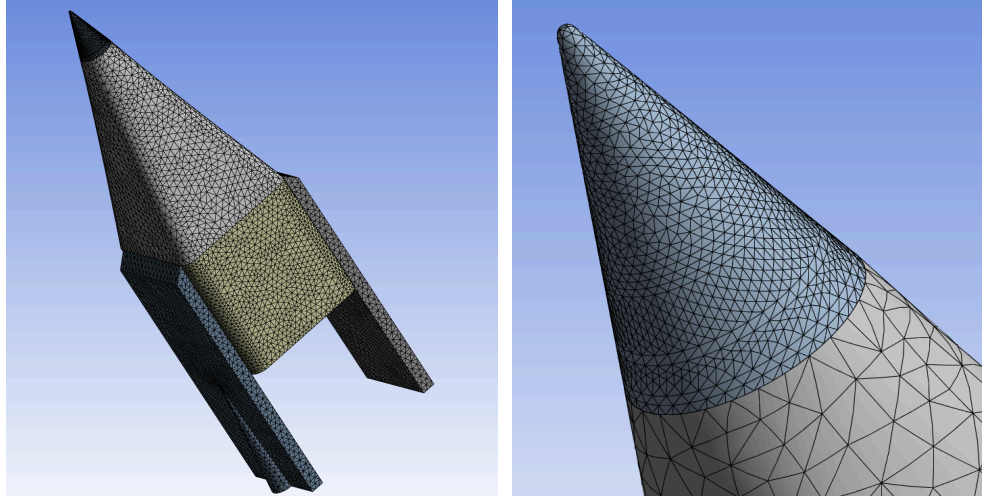
Figure 28: HEDGE Mesh for FEA

The model was simplified to address mesh failures that occurred on internal electrical components of HEDGE. All electronics were replaced with a copper block, and because of symmetry, two fins were removed to increase the speed of computations. Main differences include the shape of the fins and the lack of hinges. We expect temperatures along the fins and hinges to be higher than the results of our simulation. Auto-meshing was suitable for our model, though we increased the refinement from 1 to 3 to improve the accuracy of our results.

Convection and radiation were applied as thermal boundary conditions, and the same pressures utilized in hand calculations were applied as structural boundary conditions. A fixed support was applied to the tip of the nose cone in order to analyze deformation. For radiation, HEDGE will radiate to an ambient space temperature of approximately 2.7 K, and the emissivity of Inconel 718 was estimated to be 0.2438 (Keller, 2015). The simulation started from an initial temperature of 298.15 K. Convection in Region 1 of Figure 25 was defined by a convection coefficient (h) of 2,676,600 W/m^2K and an adiabatic wall temperature (Taw) of 23,170 K. Region 2 was defined by h = 19.53 W/m^2K and Taw = 14,010 K. Region 3 was defined by h = 2.638 W/m^2K and Taw = 13.800 K. Derivations for these values can be found in Appendix G. With these conditions, the FEA solution failed. In reality, heat transfer decreases across the nose cone, but the high h for Region 1 reflects only the stagnation point. The following averages for across the region were used to correct ANSYS errors: h = 8500 W/m^2K and Taw = 14500 K. With all other boundary conditions unchanged, the simulation yielded the temperature distribution shown in Figure 29.
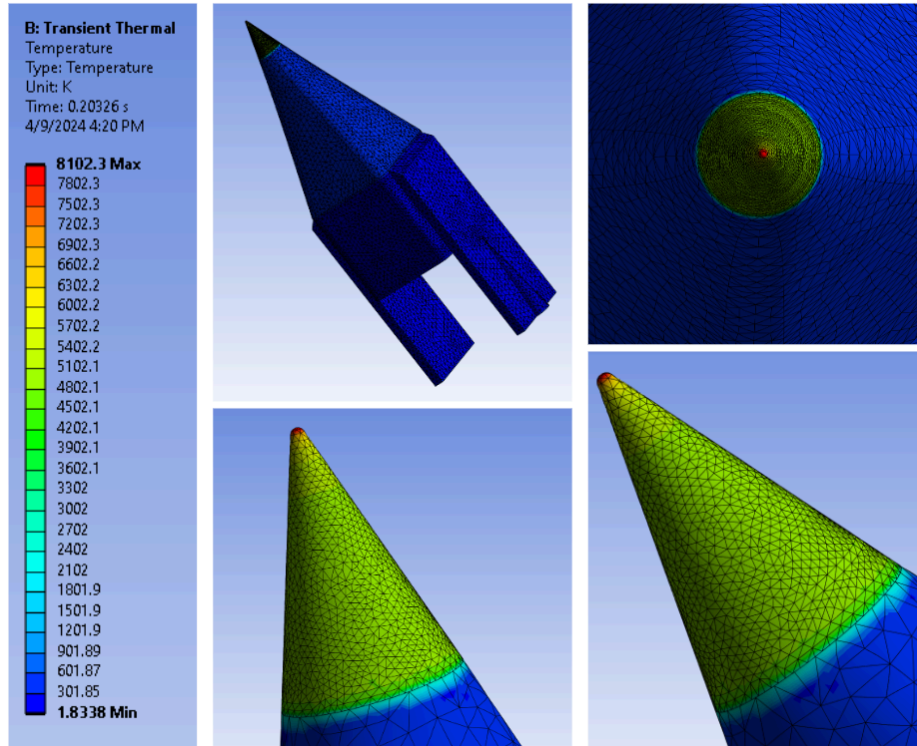
Figure 29: HEDGE FEA Temperature Solution

The total deformation solution for the transient structural analysis of HEDGE encountered computational errors, but partial results are displayed in Figure 30. We both anticipate and require the deterioration of structural components during reentry, and structural failures make sense when temperatures far exceed Inconel 718's melting point. The transient analysis was initially set at 1 second, and in the partial solution, total deformation reached 13.57 mm. The time could not be increased beyond 1 second with the present computational errors, so design changes would be necessary to increase the life of the structure. Additions to the thermal protection system, such as additional layers of Zirconia coating on the nose cone and other paints or films, would prevent immediate structural damage. Increasing the bluntness of the nose cone would also improve its performance, as the sharp point both melts and deforms the fastest.
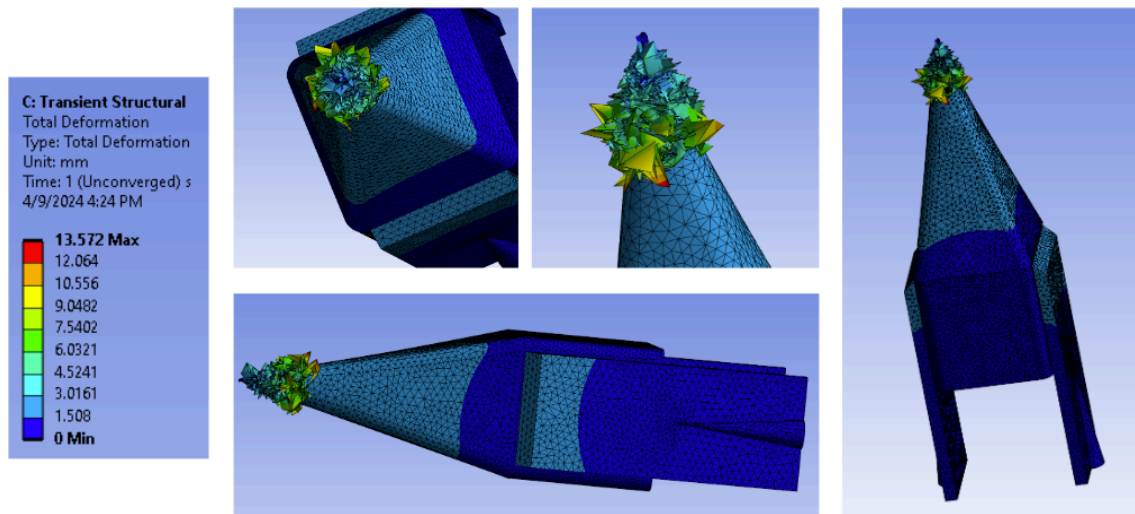
Figure 30: HEDGE FEA Total Deformation Solution

The CFD simulation discussed in the ADACs section of the thesis was also utilized to evaluate analytical calculations concerning oblique shockwave and expansion fan effects on the pressure distribution over HEDGE. The flow properties, material specifications, and simulation type remained the same (Table 5). Data points containing pressure values along the HEDGE body were plotted and compared to the analytical values obtained above. The analytical model was expanded to include the fin seen in the 2D CFD model (Figure 19). This fin results in a second oblique shockwave with a turn angle of 33 degrees. The result of this comparison and region definitions are shown in Figure 31. It's important to note that the analytical solution assumes constant pressure across each of the four regions annotated in Figure 31, whereas the CFD model calculates many pressure points across each region. Both sets of data start at an atmospheric pressure of 1.1 Pa, just before the nose of HEDGE (Region 1). Point S denotes the nose of HEDGE, where a stagnation point occurs. The analytical value was around 100 Pa above the CFD value and was found using the Rayleigh Pitot tube relation (Eqn. 5). The next analytical value represents the pressure in region 2 between the first oblique shock and the expansion fan. As shown on the plot, this value falls a bit below what is predicted by CFD. The third analytical value is in region 3, after the expansion fan, and shows a decrease in pressure due to the expansion fan, which agrees with the CFD simulation but, again, falls below. The last analytical value lies in region 4, representing the pressure after the oblique shock at the fin, and matches well with the CFD model. Overall, the same general trend is observed for both models. Differences in the two models can be attributed to the fact that the analytical model assumes inviscid flow while the CFD model accounts for the boundary layer that forms along the HEDGE body.
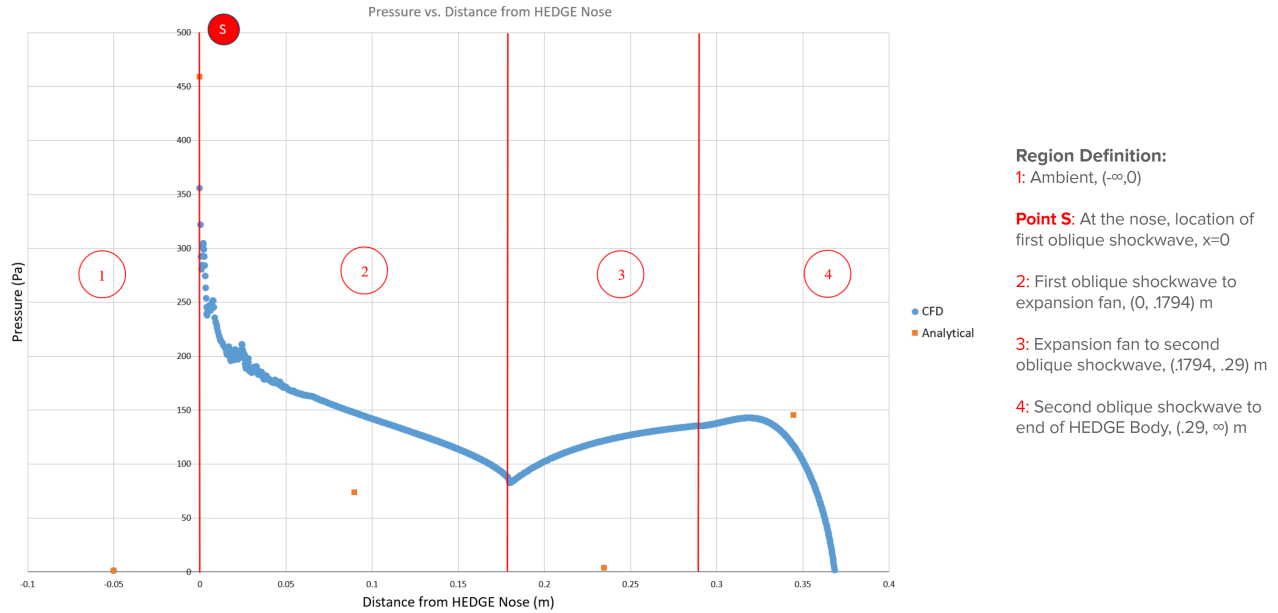
Figure 31: Comparison of 2D CFD Pressure data to Analytical Predictions along HEDGE body

$$\frac{P_{02}}{P_1} = \left[\frac{(\gamma+1)^2 M^2}{4\gamma M^2 - 2(\gamma-1)}\right]^{\frac{\gamma}{(\gamma-1)}} \left[\frac{1-\gamma+2\gamma M^2}{\gamma+1}\right] \qquad \text{Eqn. 5}$$

Components and Justification: Environment

The environment subsystem encompasses the whole of the HEDGE design, testing the entire structure under launch and reentry conditions. The environment simulations will analyze the design as a whole to see if it survives launch, and if the design fails at any point, those components will need to change.

Prototyping and Analysis: Environment

To determine if HEDGE will survive launch, a modal analysis and random vibration analysis were performed using ANSYS Mechanical. Modal analysis was initially run on a solid rectangular prism to ensure that the conditions that were imputed produced expected results. The most updated model from the structures team, which included internal components, the threaded road for the avionics board, the nose cose, the flaps, but not the solar panels, was loaded into ANSYS. Fixed supports were added to the edges and bottom and top faces, which can be seen in Figure 32, of the body of HEDGE to simulate the support it would get from the launch canister. Also in Figure 32 the final mesh is seen. The mesh is much coarser than what is ideal, and refining the mesh is something that can be explored by the next class.
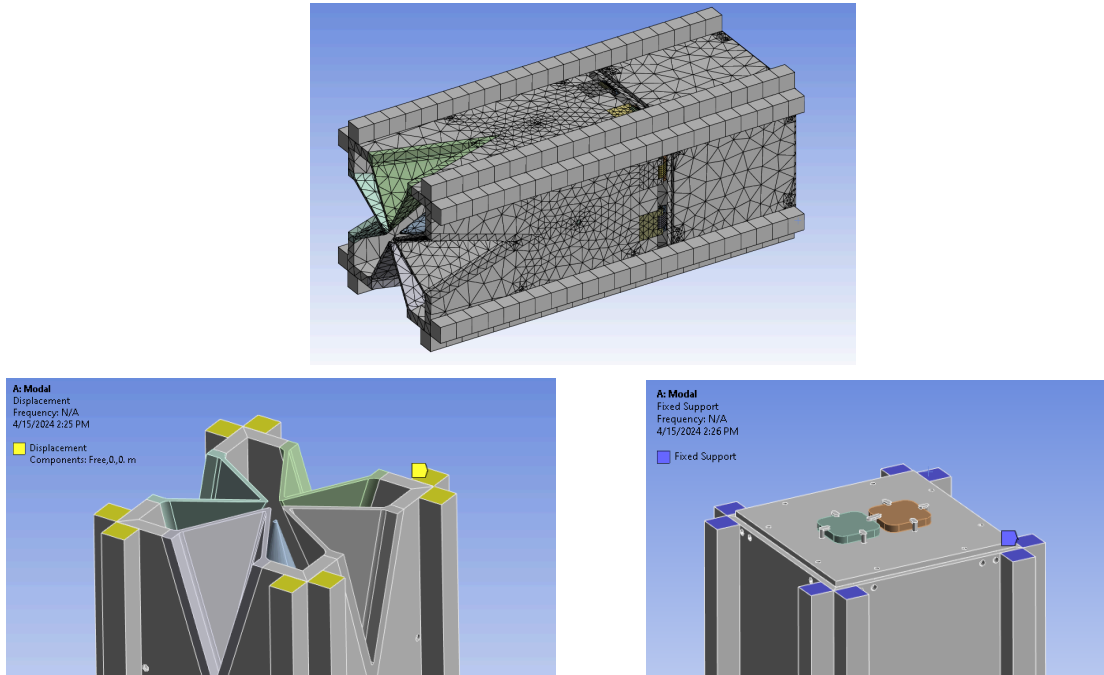
Figure 32: HEDGE Modal Analysis Mesh and Boundary Conditions

A random vibration analysis was performed. Data from the SpaceX Falcon 9 User Handbook was entered as the value of power spectral density G acceleration, loaded in the axial direction, which is a function that represents random vibration in the frequency domain, and can be seen below in Table 7.

Table 7: Falcon 9 Random Vibration Maximum Predicted Environment

Frequency (Hz)	Acceleration (G^2/Hz)
20	0.0044
100	0.0044
300	0.01
700	0.01
800	0.03
925	0.03
2000	0.00644

Afterwards, the model was solved for directional deformation. The deformation in the y-direction was the highest and those results can be seen in Figure 33. The x-direction deformation was about 9x smaller than the y-direction deformation. The figure illustrates how

much different components of the model will deform in meters under the conditions loaded in from the Falcon 9 Handbook.
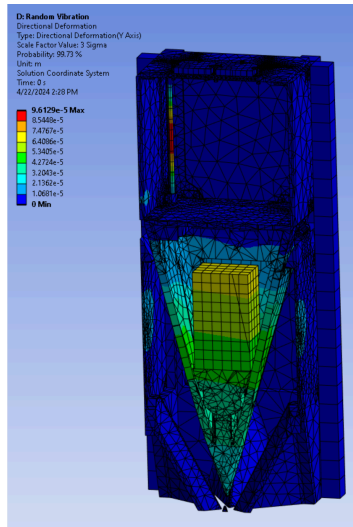

Figure 33: Y-Axis Deformation for Random Vibration Analysis

It is seen that the parts that undergo the most deformation during launch are the internal components, particularly the battery pack. These components still only deform by approximately 0.09 millimeters, which is very small and an acceptable amount of movement so that the components will not sustain damage. The maximum stress is estimated to be 30 MPa, which is less than the 600 MPa yield strength of inconel. This model does not include the solar panels, so future simulations should be reworked to include them for the most accurate launch simulation.

To further identify how HEDGE will react to the loads during launch, a transient structural simulation was run, inputting data from a Falcon Heavy launch (Figure 34). The accelerations from this graph were increased by a factor of 3 to match what would be experienced by a payload under 4000 lbs on a Falcon 9 rocket.
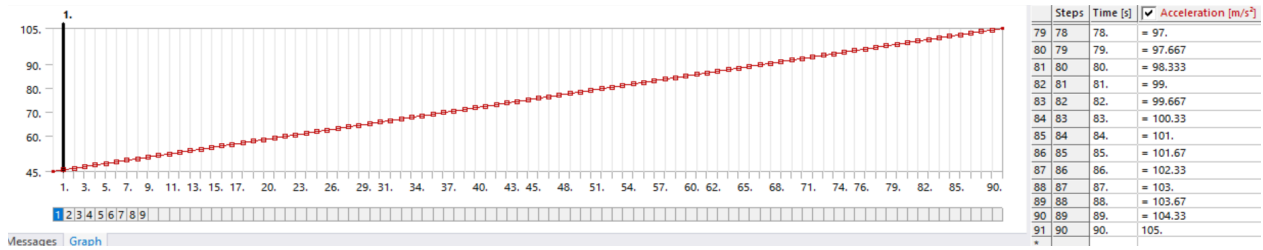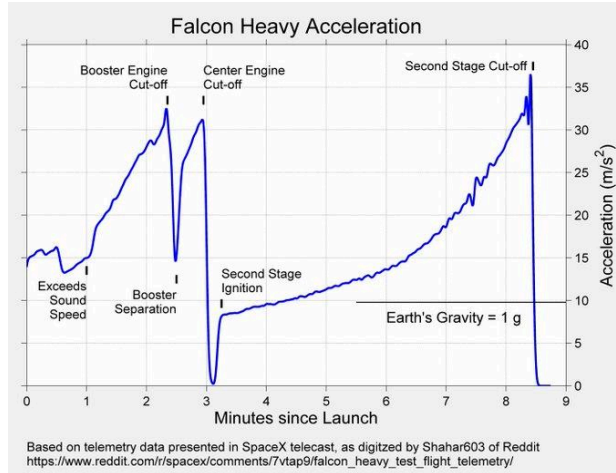
Figure 34: Falcon Heavy Acceleration
The top image presents the data received from SpaceX telemetry for the Falcon Heavy and the bottom image is that data entered into ANSYS Mechanical for the transient structural analysis.

The results from this analysis can be seen in Figure 35, and the measured equivalent stress ranged from 2.9584E-6 Pa to 26428 Pa, which is less than the 600 MPa yield strength for inconel. The majority of the design experienced the minimum equivalent stress, there was a single screw that experienced the maximum stress.
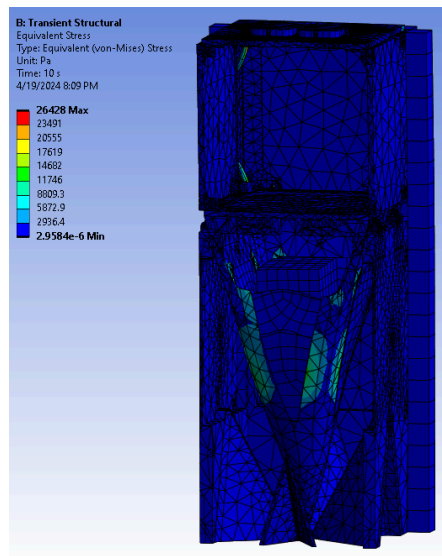

Figure 35: Transient Structural Analysis (Equivalent Stress) with Falcon Heavy Acceleration

44

Continuing to use the Falcon Heavy data, another transient structural analysis was run, this time looking at total deformation in meters over the full 90 second launch period. The results of this can be seen in Figure 36. Here it is seen that the majority of HEDGE's structure does not deform over the course of launch, but some of the screws will deform a fraction of a millimeter.
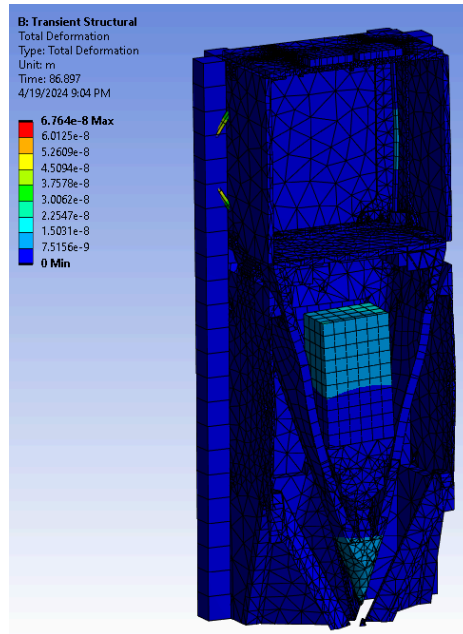

Figure 36: Transient Structural Analysis (Total Deformation) with Falcon Heavy Acceleration

Conclusion

The HEDGE mission is designed to be a proof of concept mission to demonstrate the feasibility of using CubeSats as a means of low cost hypersonic flight testing. Hypersonic conditions are extremely challenging and expensive to generate, especially with traditional flight methods. By using a CubeSat as an alternative, HEDGE offers the ability to achieve hypersonic flight conditions at a much lower cost. Hypersonic flight testing allows for the advancement of a key technology and this aligns our project with DOD and with NASA goals.

The HEDGE mission utilizes undergraduate students divided into six different functional teams. This emphasizes real world systems engineering skills and requires collaboration between all students in the class. Each functional team has a specific role in the mission and has accomplished many different tasks throughout the semester. The program management team has ensured timely progress on deliverables and ensured teams are up to date throughout the year, and next year's program management team will continue to do so.

The study to date has been successful but further work is recommended. The structures and integration team should work towards finalizing the designs implements that were put into place this semester as well as testing certain concerns related to reentry and deployment of the spacecraft. By conducting tests and finalizing the design, the team can work towards getting the spacecraft prototype built from its intended material, Inconel 718.

The software and avionics team should further the development from this year's

prototype by configuring it to both the new EnduroSat OBC and the finalized components.

The environment team should take what was learned from the random vibration analysis, and iterate the simulations with more updated models and add the solar panels to the design, in addition to further material testing. The thermal team should utilize the CFD simulation from this year and through further post-processing work, look to create the resulting surface temperature and heat transfer contours. The power team should continue to update the power budget with the finalized components, construct the auxiliary battery pack, and integrate all electrical components together.

The Attitude Determination and Controls Systems and Orbits team should continue to perform trajectory and connectivity analyses using STK. They should continue to perform updated CFD analyses as the structures change to ensure static stability during reentry, and should attempt to perform 3D CFD analysis. The attitude determination algorithm should be refined and prepared to take pressure data from HEDGE after its flight.

The Communications team should continue to calculate the link budget using STK, updating the parameters of the satellites, transceiver, receivers, and antenna with more accurate inputs. Systems Integration Review (SIR)

Currently HEDGE is undergoing its Critical Design Review (CDR) to determine if the design is mature enough to begin fabrication and testing. Due to the fact that HEDGE does not currently meet the mission objectives due to power management and use, it is not mature enough to begin fabrication and testing. With that said, once these issues are resolved in the near future, it should be ready. This is a problem that next year's class is expected to address. This will most likely be resolved through one of the solutions involving the GNSS which were detailed earlier in this paper. We expect that the design components and systems will be finalized, although more work will be needed regarding integration of system components. After completion of the critical design review next year's capstone class will conduct a Systems Integration Review (SIR) and begin fabrication and testing.

References

Ansys STK | Digital Mission Engineering Software. (n.d.).
https://www.ansys.com/products/missions/ansys-stk

Hiester, N. K., & Clark, C. F. (1966). Feasibility Of Standard Evaluation Procedures For
Ablating Materials. NASA Contractor Report.
https://ntrs.nasa.gov/api/citations/19660008602/downloads/19660008602.pdf

I. V. Belokonov, I. A. Timbai and D. D. Davydov, "Passive Stabilization Systems for CubeSat
Nanosatellites: General Principles and Features," 2019 26th Saint Petersburg International
Conference on Integrated Navigation Systems (ICINS), St. Petersburg, Russia, 2019, pp. 1-7,
https://doi.org/10.23919/ICINS.2019.8769434

Keller, B. P., Nelson, S. E., Walton, K. L., Ghosh, T. K., Tompson, R. V., & Loyalka, S. K.
(2015). "Total hemispherical emissivity of Inconel 718." *Nuclear Engineering and
Design*, Vol. 287, pp. 11-18, https://doi.org/10.1016/j.nucengdes.2015.02.018

Lee, S., Yang, Y. and Kim, J.G. (2023), "Evaluation of Fay and Riddell formula under hypersonic flight
conditions", *International Journal of Numerical Methods for Heat & Fluid Flow*, Vol. 33 No. 1,
pp. 14-41. https://doi.org/10.1108/HFF-01-2022-0051

McInnes, C. R. (2011). A passive de-orbiting strategy for high altitude CubeSat missions using a
deployable reflective balloon. *Journal of Guidance, Control, and Dynamics*, 34(2),
388-395.

Office of Engineering and Technology. (2013, March 15). *Guidance on obtaining licenses for
small satellites.* Federal Communications Commission.
https://docs.fcc.gov/public/attachments/DA-13-445A1.pdf

"Payload User's Guide." *Rocket Labs*, 1 Nov. 2022,
www.rocketlabusa.com/assets/Uploads/Electron-Payload-User-Guide-7.0.pdf.

Prado, A. (2018). Conceptual Study of De-Orbiting Small Satellites Using a Parasitic Drag
Device. Presented at the Symposium on Space Science and Technology for Sustainable
Development in the Americas, Brazil.
https://www.unoosa.org/documents/pdf/psa/activities/2018/Symposium_Brazil_BSTI/pre
sentations/poster/P07_PRADO_ANTONIO.pdf

Properties of Standard Atmosphere. (n.d.). Rocket and Space Technology. Retrieved April 15,
2024, from http://www.braeunig.us/space/atmos.htm

Raydugin, Yuri. "Consistent application of risk management for selection of engineering design options in mega-projects." International Journal of Risk and Contingency Management, vol. 1, no. 4, 1 Oct. 2012, pp. 44–55, https://doi.org/10.4018/ijrcm.2012100104.

Riot, Vincent J., Simms, Lance M., & Carter, Darrell. (2021). Lessons Learned Using Iridium to Communicate with a CubeSat in Low Earth Orbit. United States. https://www.osti.gov/biblio/1770026

S3VI, Small Spacecraft Systems Virtual Institute. (2023). *NASA SSRI knowledge base, Resources for smallsat success, Licensing and regulations.* National Aeronautics and Space Administration. https://s3vi.ndc.nasa.gov/ssri-kb/topics/8/

Starship's Third Flight Test. (2023). SpaceX. Retrieved March 28, 2024, from https://www.spacex.com/launches/mission/?missionId=starship-flight-3

Weston, S. (Ed.). (2024, February 23). 8.0 Small Spacecraft Avionics. NASA. https://www.nasa.gov/smallsat-institute/sst-soa/small-spacecraft-avionics/#8.2

What is a link budget?. What Is a Link Budget? - MATLAB & Simulink. (n.d.). https://www.mathworks.com/discovery/link-budget.html#:~:text=A%20link%20budget%20is%20a,stage%20of%20the%20transmission%20path.

White, F. M., & Majdalani, J. (2022). *Viscous Fluid Flow.* McGraw Hill. ISBN: 978-1-260-59780-6

2022-2023 Spacecraft Design Team. (2023, April 12). *HEDGE Thesis*. University of Virginia

Appendices

Appendix A: Teams and Roles

To organize this technical project, the class has been split into six functional teams, composed of undergraduate aerospace and mechanical engineering majors. The groups are as follows: 1) Program Management, 2) Structures & Integration, 3) Communications, 4) Software & Avionics, 5) Power, Thermal & Environment; and 6) Attitude Determinations and Control Systems & Orbits (ADACS). The table below shows the functional team assignments for the 2023-2024 Capstone team.

Functional Teams	Team Members (Bold Indicates Team Leader)
Program Management	**Najarie Williams**, Griffin Dewey, Brett Schriever, Owen Solomon
Communications	**Tyler Spittle**, Kate Wilkins, Sean Jolly, Emmanuel Kenscoff, Temidayo Akinbi
Software and Avionics	**Amy Paz Cuervo**, William Plunkett, Brandol Galicia, Morgan Myers, Timothee Kambouris
Power, Thermal, and Environment	**Katie Borland**, Troy Daigneau, Juan Victor Corsino, Jennifer Farfel, Lucas Haddock, Owen Tuohy
Attitude Determination and Control System (ADACS) and Orbits	**Justin Carroll**, Samuel Falls, Isaac Farias, Rishab Gopisetti
Structures and Integration	**Benjamin Koeppen**, William Jones, Arlee Christian, Lobsang Dawa, Ian McAninley
Electrical and Computer Engineering	**Luke Bulmer**, Justin Casotti, Daniel Goodman, Connor Schichtel

Appendix B: Full Budget

Team	Components	Quantity	Cost Per Unit	Total Cost
ADACS	316 Stainless Steel Tubing (3 ft)	1	$47.70	$47.70
	Idex Chromatography Tubing, Natural ETFE (5ft)	1	$39.70	$39.70
	Compression Spring (Pack of 12)	1	$8.27	$8.27
Communications	Iridium 9603 Transceiver	2	$199.00	$398.00
	Taoglas Iridium Patch Antenna	1	$8.79	$8.79
	Iridium Satellite Constellation License	12	$32.50	$390.00
	EnduroSat GNSS Patch Antenna	1	$4,700.00	$4,700.00
Software and Avionics	Endurosat OBC	1	$5,100	$5,100.00
	SDK License	1	$6,600	$6,600.00
	Inconcel Type K Thermocouple	10	$26.68	$266.80
	Kulite XCE-80 Pressure Transducer	10	$1,555	$15,550.00
Power, Thermal, and Environment	EnduroSat EPS I Plus	1	$5,800.00	$5,800.00
	EnduroSat 1U Solar Panel X/Y	3	$2,600.00	$7,800.00
	EnduroSat 1U Solar Panel X/Y w/ Remove Before Flight Pin	1	$2,700.00	$2,700.00
	Ablative Panels	4	$500.00	$2,000.00
Structures and Integration	Inconel Parts (Some Machining Included)	1	$9,239.88	$9,239.88
	EnduroSat 1U CubeSat Structure	1	$1,900.00	$1,900.00
	Test Panels	4	N/A	N/A
	6061 Aluminum Sheet 4"x4"	5	$40.28	$201.40
Miscellaneous	FCC Licensing	1	$140	$140
	Other Materials and Supplies	1	$10,000.00	$10,000.00
			Total	**$72,890.54**

Appendix C: Risk Management

The following chart explains the risk management scale used by this team. Each risk is measured by the probability of occurrence, multiplied by the severity of the impact it would have on the project objectives, should it occur.

		Impact on Project Objectives				
		Slight degradation of element performance	Minor effect on system performance	All design and operating margins eliminated	Substantial effects on performance	System objectives and requirements not achieved
		Very low (1)	low (2)	Medium (3)	High (4)	Very High (5)
Probability of Occurrence	Almost Certain (5)	5	10	15	20	25
	Likely (4)	4	8	12	16	20
	Possible (3)	3	6	9	12	15
	Unlikely (2)	2	4	6	8	10
	Rare (1)	1	2	3	4	5

Adapted from Raydugin (2012)

Appendix D: Power Budgets

Total Power Available (Watt Hours)

Component	Power Available (Wh)
Solar Panel Generation	497.7
EPS Built in Battery	20.8
Auxiliary Battery	51.8
Dormant Battery Drain for Auxiliary*	-18.65
Dormant Battery Drain for EPS*	-7.45
Total Power Available for Mission	543.9

*Battery drain calculated assuming loss of 3% per month when dormant for 1 year

Power Budget During Orbit

*Total power consumption calculated assuming 16 day orbital period. This slide shows that power requirements for a 16 day mission are met when GNSS is active for 50% of the time but not 100%

Voltage	Component	Subsystem	Duty Cycle (%)		Current Draw (W)		Average Current Draw (W)	Total Power Draw (Wh)
			Idle/Low	Operation	Idle/Low	Operation		
3.3	EnduroSat OBC 1 w/GNSS at 0%	Software and Avionics	100	0	0.195	1.420	0.195	74.88
	EnduroSat OBC 1 w/GNSS at 50%	Software and Avionics	50	50	0.195	1.420	0.808	310.272
	EnduroSat OBC 1 w/GNSS at 100%	Software and Avionics	0	100	0.195	1.420	1.420	545.28
5	RockBLOCK 9603	Communications	99.86	0.14	0.2	2.25	0.2029	77.902
10	Kulite XCE-80 Pressure Transducer (x4)	Software and Avionics	100	0	0	~0	~0	~0
N/A	Thermocouples (x4)	Software and Avionics	100	0	0	~0	~0	~0
	Analog to Digital Converter	Software and Avionics	100	0	0	~0	~0	~0
	EnduroSat EPS 1-Plus	PTE	0	100	0	0.075	0.075	28.8
Total Power Draw w/ GNSS at 0%								179.58
Total Power Draw w/ GNSS at 50%								416.97
Total Power Draw w/ GNSS at 100%								651.98
TOTAL POWER AVAILABLE FOR MISSION								543.9

Power Budget During Re-Entry

*Total power consumption calculated assuming 1 hour re-entry time. This slide shows that if the GNSS is active 50% of the time, power requirements will be met when accounting for re-entry power consumption.

Voltage	Component	Subsystem	Duty Cycle (%)		Current Draw (W)		Average Current Draw (W)	Total Power Draw (Wh)
			Idle/Low	Operation	Idle/Low	Operation		
3.3	EnduroSat OBC 1 w/GNSS	Software and Avionics	0	100	0.195	1.420	1.420	1.420
5	RockBLOCK 9603	Communications	87.5	12.5	0.2	2.25	0.456	0.456
10	Kulite XCE-80 Pressure Transducer (x4)	Software and Avionics	0	100	0	~0	~0	~0
N/A	Thermocouples (x4)	Software and Avionics	0	100	0	~0	~0	~0
	Analog to Digital Converter	Software and Avionics	0	100	0	~0	~0	~0
	EnduroSat EPS 1-Plus	PTE	0	100	0	0.075	0.075	0.075
Total Power Draw During Re-Entry								1.951
Power Available if GNSS is on 50% during orbit		543.9 - 416.97						126.93
Power Remaining		126.93-1.951						124.97
Mission Factor of Safety		543.9/(543.9-124.97)						1.298

Total Power Available for 59.5 Hour Mission

Component	Power Available (Wh)
Solar Panel Generation	77.124
EPS Built in Battery	20.8
Auxiliary Battery	51.8
Dormant Battery Drain for Auxiliary*	-18.65
Dormant Battery Drain for EPS*	-7.45
Total Power Available for Mission	**123.62**

*Battery drain calculated assuming loss of 3% per month when dormant for 1 year

Power Budget Assuming 100% GNSS Use

*Assuming re-entry phase consumption is still 1.951 Wh and a total mission factor of safety of 1.2. This slide shows power requirements will be met when mission duration is limited to 59.5 hours.

Voltage	Component	Subsystem	Duty Cycle (%)		Current Draw (W)		Average Current Draw (W)	Total Power Draw (Wh)
			Idle/Low	Operation	Idle/Low	Operation		
3.3	EnduroSat OBC 1 w/GNSS at 100%	Software and Avionics	0	100	0.195	1.420	1.420	84.49
5	RockBLOCK 9603	Communications	99.86	0.14	0.20	0.45	0.2029	12.07
10	Kulite XCE-80 Pressure Transducer (x4)	Software and Avionics	100	0	0	~0	~0	~0
N/A	Thermocouples (x4)	Software and Avionics	100	0	0	~0	~0	~0
	Analog to Digital Converter	Software and Avionics	100	0	0	~0	~0	~0
	EnduroSat EPS 1-Plus	PTE	0	100	0	0.075	0.075	4.46
Power Required for Re-Entry								1.951
Total Power Draw w/ GNSS at 100%								**102.98**
Total Power Draw w/ Factor of Safety of of 1.2		102.98 x 1.2						**123.57**
TOTAL POWER AVAILABLE FOR MISSION								123.62

Appendix E: Thermal Calculations

1: Compressible Flow Calculator Results

Oblique Shock Calculator

Input: $M_1 = 20$

$M_2 = 5.3316$

$p_2/p_1 = 66.8781$

$p_{02}/p_{01} = 0.01080$

$p_2/p_{02} = 0.001294$

$T_2/T_1 = 12.116$

Isentropic Flow Calculator

Input: $M_2 = 5.3316$

$p_2/p_{02} = 0.001294$

$p_3/p_{03} = 0.00006321$

$T_2/T_{02} = 0.14958$

$T_3/T_{03} = 0.0635$

Prandtl-Meyer Table

Input: $M_2 = 5.3316$

$v_2 = 79.8628°$

$v_3 = 97.8928°$

$M_3 = 8.614095$

$$p_3 = p_3/p_{03} * p_{03}/p_{02} * p_{02}/p_2 * p_2/p_1 * p_1 = 3.59 \text{ Pa}$$

$$T_3 = T_3/T_{03} * T_{03}/T_{02} * T_{02}/T_2 * T_2/T_1 * T_1 = 1021.7 \text{ K}$$

2: Van Driest Model

Source: White, F. M. and Majdalani, J., 2022

$$Q = C_h * (\rho_e * U_e * C_{pe} * (T_{aw} - T_w))$$

C_h = local Stanton number
ρ_e = post-shock density
U_e = post-shock velocity
C_{pe} = post-shock specific heat
T_{aw} = adiabatic wall temperature
$\quad = T_e + r(U_e^2/2C_{pe})$
T_w = wall temperature

Assumptions:
$r(Pr) = 0.84771$
$T_w = 1273.15 \text{ K}$
$R = 287 \text{ J/kg*K}$

Region 2 Aerodynamic Properties

Te =	2406.7 K
Taw =	14011.2 K
Tw =	1273.15 K
L =	.025 m
μe =	7.7154E-5 Pa-s
Cpe =	1271.66 J/kg

$\rho_e = P/R*Te = 0.00010651 \text{ kg/m}^3$

$U_e = M \sqrt{\gamma*R*Te} = 5242.9 \text{ m/s}$

$Re = \rho_e*U_e*L/\mu_e = 180.94$

Region 3 Aerodynamic Properties

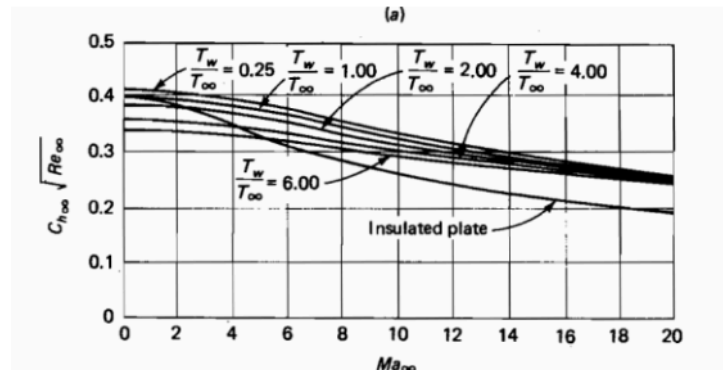|	
Te =	1021.7 K
Taw =	13800.8 K
Tw =	1273.15 K
L =	.05 m
μe =	4.3885E-5 Pa-s
Cpe =	1144.97 J/kg

$\rho_e = P/R*Te = 0.000012243 \text{ kg/m}^3$

$U_e = M \sqrt{\gamma*R*Te} = 5501.84 \text{ m/s}$

$Re = \rho_e*U_e*L/\mu_e = 76.745$

$T_w/T\infty_2 = 0.5$

$C_{h2} = 0.37/\sqrt{Re_2} = 0.0275$

$T_w/T\infty_3 = 1$

$C_{h3} = 0.3/\sqrt{Re_3} = 0.0342$

$Q_2 = 2.48753 * 10^5 \text{ W/m}^2$

$Q_3 = 3.3043 * 10^4 \text{ W/m}^2$

Source: Lee, Yang, and Kim, 2023

$$Q = 0.763 P_r^{-0.6}(\rho_w \mu_w)^{0.1}(\rho_e \mu_e)^{0.4}[1 - \frac{h_R}{h_e}](h_e - h_w)\sqrt{\beta}$$

$$\beta = \frac{1}{R}\sqrt{\frac{2(p_e - p_\infty)}{\rho_e}}$$

$ho\infty = (M\sqrt{\gamma R T\infty})^2/2$

subscript e = boundary layer edge
subscript ∞ = free stream
subscript w = surface

Pr = 0.7
Rconst = 287 J/kg*K
M = 20
Tw = 1273.15 K
T∞ = 198.64 K
P∞ = 1.1 Pa
R = 0.00125 m

Pr = Prandtl number
ρ = density
μ = viscosity
h = enthalpy
u = velocity
β = velocity gradient
R = nose cone radius
P = pressure
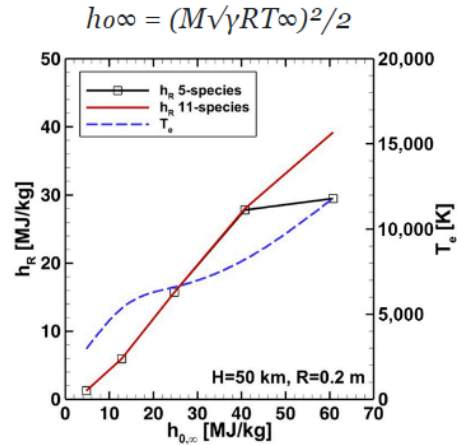
Appendix F: Burn-up Calculations

Stagnation point:

Temp increase/second = (Q * nose cone area) / (nose cone mass * inconel specific heat)
Burn-up Time = inconel melting point / (temp increase/second)

Q = 4.46434 * 10⁶ W/m²
Inconel melting point = 1610 K
Inconel specific heat capacity = 0.435 J/g-C
Nose cone mass = 80.262 g
Nose cone area = 0.00155227941653 m²

Temp increase/second = 198.485 K/s

Time until melt = 8.111 s

Inconel Panels:

Temp increase/second = (Q * panel area) / (panel mass * inconel specific heat)
Burn-up Time = inconel melting point / (temp increase/second)

Region 2 Properties, Inconel Panel ONLY

Known Te, Taw, Tw, ρe, μe, Cpe, Ue
L = 0.11165 m
Re = ρe*Ue*L/μe = 808.095
From Van Driest graph:
Tw/T∞ = 0.5
Ch = 0.37/√Re = 0.01302

Q = 1.17735 * 10⁵ W/m²

Inconel melting point = 1610 K
Inconel specific heat capacity = 0.435 J/g-C
Panel mass = 10.7706 g
Panel area = 0.00247519 m²

Temp increase/second = 62.2 K/s

Time until melt = 25.9 s

Teflon Panels:

Mass loss rate $= 0.0076*(Q)^{0.55}(P_{02})^{0.27}$
Burn-up Time = (panel thickness)*(panel density)/mass loss rate

Region 2 Properties, Teflon Panel ONLY

Known Te, Taw, Tw, ρe, μe, Cpe, Ue
L = 0.11165 m
Re = ρe*Ue*L/μe = 808.095
From Van Driest graph:
    $Tw/T\infty$ = 0.5
    Ch = 0.37/√Re = 0.01302

    Q $= 1.17735 * 10^5$ W/m²

Total pressure after the shock p_{02} = 56,852 Pa
Panel thickness = 5 mm
Panel density = 2200 kg/m³

Mass Loss Rate = 89.866
kg/m² per second

Time Until Ablation = 0.12241 s

Phenolic-Nylon Panels:

Mass loss rate $= 0.0017*(Q)^{0.56}(P_{02})^{0.13}$
Burn-up Time = (panel thickness)*(panel density)/mass loss rate

Region 2 Properties, Panel ONLY

Known Te, Taw, Tw, ρe, μe, Cpe, Ue
L = 0.11165 m
Re = ρe*Ue*L/μe = 808.095
From Van Driest graph:
    $Tw/T\infty$ = 0.5
    Ch = 0.37/√Re = 0.01302

    Q $= 1.17735 * 10^5$ W/m²

Total pressure after the shock p_{02} = 56,852 Pa
Panel thickness = 5 mm
Panel density = 1201.38 kg/m³

Mass Loss Rate = 4.878 kg/m² per second

Time Until Ablation = 1.2313 s

Appendix G: FEA Boundary Condition Calculations

Boundary Conditions

Thermal
Initial temperature: 25 C == 298.15 K

Convection 1
- h = 2676558 W/m²K
- Taw = 23174 K

Convection 2
- h = 19.53 W/m²K
- Taw = 14011 K

Convection 3
- h = 2.638 W/m²K
- Taw = 13800 K

Radiation
- Emissivity = 0.24375
- Ambient temperature = 2.7 K

Structural
Fixed support at tip of nose cone.

Pressure 1 = 1.1 Pa
Pressure 2 = 73.557 Pa
Pressure 3 = 3.59 Pa

Convection 1

Taw = T_0 = 23174 K

$T_0 = T + \frac{v^2}{2Cp}$, where T = 198.64 K, C_p = 1008 J/kg, and M = 20

h = 2676558 W/m²K

$h = \frac{Q}{A(T_s - T_b)}$, where Q = 4.46434*10⁶ W/m², A = 0.00155 m², T_s = 1273.15 K, and T_b = 198.64 K

Convection 2

$h = Ch \cdot \rho \cdot u \cdot Cpe$,
where Ch = 0.0275, ρ_e = 0.0001065 kg/m³, u_e = 5243 m/s, Cpe = 1272 J/kg

Convection 3

$h = Ch \cdot \rho \cdot u \cdot Cpe$,
where Ch = 0.0342, ρ_e = 0.0000122 kg/m³, u_e = 5502 m/s, Cpe = 1145 J/kg

Appendix H: Attitude Determination Algorithm

The following pseudocode uses one pressure transducer's reading to estimate the crafts' angle of attack. Transducers on opposite sides of HEDGE should predict the same angle of attack.

 # Take in data:
θ = 14.123°   *#Physical property of Hedge*
Get altitude (*z*), velocity (*u₁*) from GPS
Reference lookup table to get P_1, T_1 from standard atmosphere as a function of altitude
M_1 = u_1/sqrt(1.4*287*T_1)

Measure P_2 using pressure transducer

$P = P_2/P_1$ *# we use pressure ratio for all calculations*
#Classify flow conditions
if(P<1)

   #Prandtl-Meyer Fan

   $$M_2 = \sqrt{5((\tfrac{1}{P})^{.2857}(1 + .2M_1^2) - 1)}$$
   $$\beta_0 = v(M_2) - v(M_1)$$
   $\alpha = \beta_0 + \theta$

else

   $$M_{n,1} = \sqrt{.8571P + .1429}$$

   $$M_{n,2} = \sqrt{\frac{1 + .2M_{n,1}^2}{1.4M_{n,1}^2 - .2}}$$

   $$M_{t,1} = \sqrt{M_1^2 - M_{n,1}^2}$$

   $$\beta_1 = arcsin(\frac{M_{n,1}}{M_1}) - arctan(\frac{M_{n,2}}{M_{t,1}})$$

   #We know we have an oblique shock, but we need to figure out which side we're on
   if($\beta_1 < \theta$)   *#Low pressure side*
      $\alpha = \theta - \beta_1$
   else   *#high pressure side*
      $\alpha = \beta_1 - \theta$

end
return α

Functions:

$$v(M) = \sqrt{\frac{\gamma+1}{\gamma-1}} arctan(\sqrt{\frac{\gamma+1}{\gamma-1}(M^2 - 1)}) - arctan(\sqrt{M^2 - 1})$$

Appendix I: FCC Licensing – Special Temporary Authorization (STA) Application

STA is an online application process. Filing fees are calculated after submitting the application which must be paid within 10 days of filing.

STA Application Process: https://www.fcc.gov/applying-special-temporary-authority

Important Management Links:
- FRN Management and Payments: https://apps.fcc.gov/cores/userLogin.do
- FCC License Manager: https://wireless2.fcc.gov/UlsEntry/licManager/login.jsp
- STA Application Portal: https://apps.fcc.gov/oetcf/els/forms/StaEntry.cfm

Important Dates:

2024	Q3	**July**	**Start STA application process**
		August	
		September	**Submit STA NLT last day of September**
	Q4	October	
		November	
		December	**90-day post STA submission:** Assumption that FCC will take approximately 90 days to process. If rejected, then corrections need to be made and resubmitted.
2025	Q1	January	
		February	
		March	**90-day prior to LV integration:** STA application / revisions should be completed NLT last day of March and resubmitted
	Q2	April	
		May	
		June	
	Q3	July	Tentative LV integration
		August	
		September	

Appendix J: Mass Budget

Part	Mass (g)	% of Total Mass
316 Stainless Steel Tubing (3 ft)	14.3	0.25%
Iridium 9603 Transceiver	11.4	0.20%
2J Antenna	10.98	0.19%
ADC Board	29.55	0.51%
RockBlock	40.61	0.71%
Endurosat OBC	130	2.27%
Kulite XCE-80 Pressure Transducer	0.4	0.01%
Inconcel Type K Thermocouple	0.4	0.01%
Endurosat EPS I Plus	330	5.75%
EnduroSat 1x1 Solar Panels (Qty. 3)	132	2.30%
EnduroSat 1x1 Solar Panels with RBF	44	0.77%
6061 Aluminum Sheet 4"x4" (Qty. 6)	516	8.99%
1U CubeSat Structure	120	2.09%
Inconel Nose Cone	80.28	1.40%
Inconel Forebody	1054.23	18.37%
Inconel Fins (Qty. 4)	1906.24	33.22%
Inconel Hinges	28.34	0.49%
Test Panel (Qty. 4)	405.44	7.07%
Battery	300	5.23%
Test Panel Secure Plates	85.64	1.49%
Ballast	498.2	8.68%
Total Mass	5738.01	